COMPUTATIONAL MODAL ANALYSIS OF A LOW-PRESSURE TURBINE BLADE USING DIFFERENT MATERIALS

A Final Year Project Report

Presented to

SCHOOL OF MECHANICAL & MANUFACTURING ENGINEERING

Department of Mechanical Engineering

National University of Sciences & Technology (NUST)

ISLAMABAD, PAKISTAN

In Partial Fulfillment

of the Requirements for the Degree of

Bachelors of Mechanical Engineering

By

Shehzada Anees Khan

Ihtesham Arif

June 2021

EXAMINATION COMMITTEE

We hereby recommend that the final year project report prepared under our supervision by:

IHTESHAM ARIF 00000207935

SHEHZADA ANEES KHAN 00000212791

Titled: "***COMPUTATIONAL MODAL ANALYSIS OF A LOW-PRESSURE TURBINE BLADE USING DIFFERENT MATERIALS***" be accepted in partial fulfillment of the requirements for the award of "***BACHELORS OF MECHANICAL ENGINEERING***" degree with grade ___

Supervisor: Dr. Niaz Bahadur Khan (Assistant Professor) NUST, SMME.	Dated:
Committee Member:	Dated:
Committee Member:	Dated:

_____ _____

(Head of Department) (Date)

COUNTERSIGNED

Dated: _____ _____

(Dean / Principal)

ABSTRACT

Gas turbine engines encompass a wide range of applications ranging from electricity production to aircraft propulsion. The air is raised to a high temperature and pressure which then is fed to a turbine where it expands to a lower pressure thereby imparting rotational energy to the turbine blades. The air at exhaust produces a thrust which is utilized in applications such as a turbojet engine. The turbine may comprise of several stages depending on the intake pressure such as a high-pressure turbine stage (HPT) or a low-pressure turbine stage (LPT). The purpose of an LPT is to extract the energy remnants from the exhaust air leaving the HPT. Since the LPT intakes air at a lower pressure and a higher volume, this ultimately results in the LPT being larger in size and weight. The turbine blade therefore being larger is more prone to vibrate. These vibrations along with the combined effect of centrifugal stresses and high temperature can make the blade susceptible to failure. A solution to this problem can be achieved if the vibrational characteristics of the blade are known. This is accomplished through modal analysis that basically is a measure of structure's inherent response when subjected to vibrations. The goal of this project is to analyze the modal parameters (natural frequency, mode shape) of various materials. The analysis will be carried out computationally using a commercial FEA package such as ANSYS and the results will be validated by the values obtained from the mathematical model. The obtained values of natural frequency relate to the material stiffness and mass. These results will help us in finalizing our choice regarding the blade materials suitable for operation that not only possess high stiffness but are also light in weight thus reducing the overall turbine weight.

ACKNOWLEDGMENTS

We would first of all thank Almighty Allah, who blessed us with the energy and strength to complete all the tasks successfully.

This tiresome work surely was not possible without the continuous guidance, encouragement and technical insight of our supervisors Mr. Muhammad Usman Safdar and Dr. Niaz Bahadur Khan throughout the project.

Constant prayers, support, both emotional and practical, of our parents cannot be ignored here. We have tried our level best not to omit any topic so that you may find it easy in comprehending our work.

ORIGINALTY REPORT

We hereby declare that no portion of the work of this project or report is a work of plagiarism and the workings and findings have been originally produced. The project has been done under the supervision and guidance of Mr. Muhammad Usman Safdar and Dr. Niaz Bahadur Khan and has not been a support project of any similar work serving towards a similar degree's requirement from any institute. The originality report for our project as generated by Turnitin is provided as follows.

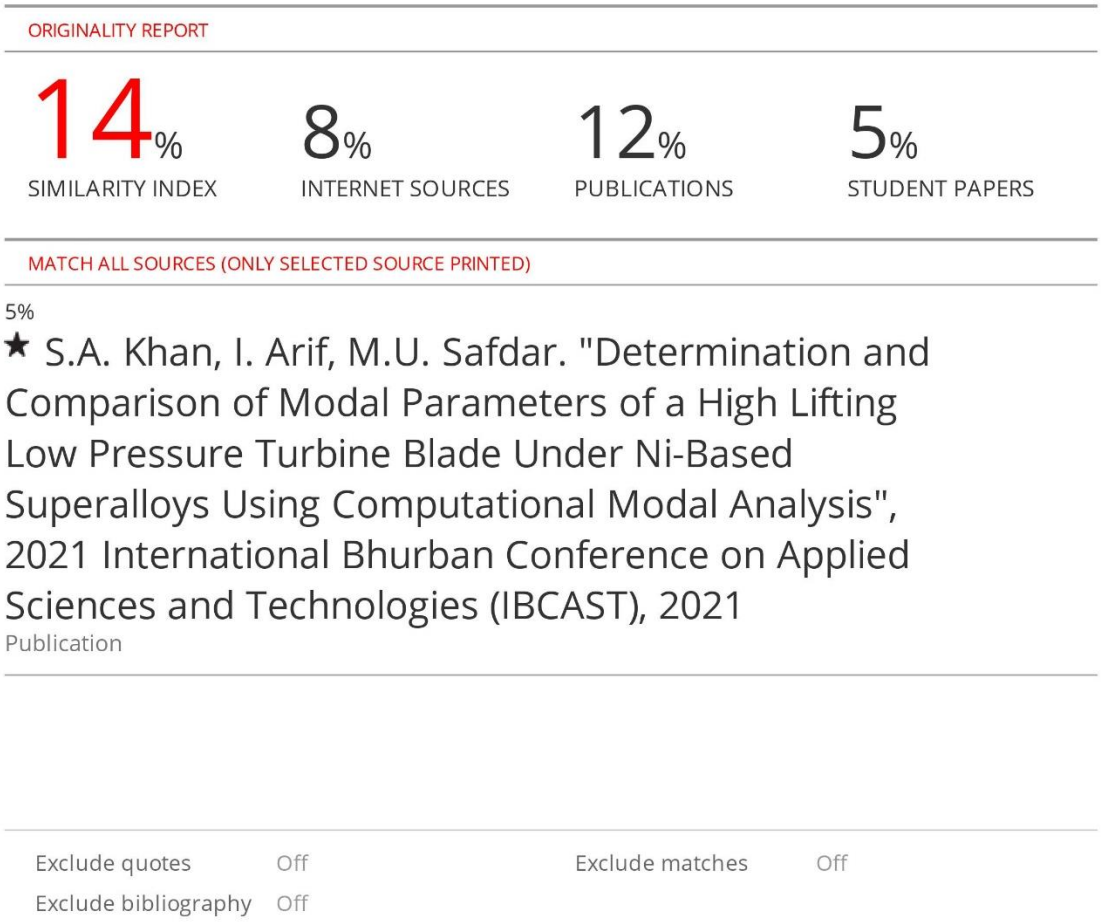

ORIGINALITY REPORT

14%	8%	12%	5%
SIMILARITY INDEX	INTERNET SOURCES	PUBLICATIONS	STUDENT PAPERS

MATCH ALL SOURCES (ONLY SELECTED SOURCE PRINTED)

5%

★ S.A. Khan, I. Arif, M.U. Safdar. "Determination and Comparison of Modal Parameters of a High Lifting Low Pressure Turbine Blade Under Ni-Based Superalloys Using Computational Modal Analysis", 2021 International Bhurban Conference on Applied Sciences and Technologies (IBCAST), 2021

Publication

Exclude quotes	Off	Exclude matches	Off
Exclude bibliography	Off		

TABLE OF CONTENTS

LIST OF TABLES

LIST OF FIGURES

ABBREVIATIONS

HPT	High Pressure Turbine
LPT	Low Pressure Turbine
FEA	Finite Element Analysis
AC	Alternating Current
Ni	Nickel
Ti-Al	Titanium Aluminide
SDOF	Single Degree of Freedom
FFT	Fast Fourier Transform
FRF	Frequency Response Function
DOF	Degrees of Freedom
EMA	Experimental Modal Analysis
TET	Turbine Entry Temperature
Co	Cobalt
Cr	Chromium
IN	Inconel
U	Udimet
Ti	Titanium
Hz	Hertz
rad/s	Radians per second
IGES	Initial Graphics Exchange Specification
RPM	Revolutions per minute
EMPR	Effective Mass Participation Ratio
PBF	Powder bed fusion
EBM	Electron beam melting
LPBF	Laser powder bed fusion
AM	Additive manufacturing

NOMENCLATURE

E	Elastic modulus	N/m^2
I	Area moment of inertia	m^4
ρ	Density	Kg/m^3
A	Cross-section area	m^2
l	length	m
ω	Natural frequency	rad/s
f	Natural frequency	1/s
m	Mass	kg
k	Stiffness	N/m
c	Damping	Ns/m
F(t)	Force	N
ζ	Damping ratio	-
Q	Quality factor	-
s	Poles of a transfer function	Rad/s
$H(w)$	Receptance	m/N
A	Scaling factor	m/Ns
n	Number of modes	
H(s)	Receptance Transfer function	

CHAPTER 1: INTRODUCTION

1.1 Gas Turbine Engines

Gas turbine engines are an important class of internal combustion engines. The incoming air is compressed as it passes through the compressor stages and the compressed air reaches the burner. Combustion in the burner produces hot gases that expand through the turbine stages, thereby driving the turbine to produce power. The mechanical power from the turbine can be used as an industrial energy source while the exhaust fluid jet can be used as a source of thrust.

Gas turbine engines are used as gas turbine power plants in land applications where the turbine drives a synchronous generator to produce AC power. On land, gas turbine power plants are mostly employed to cater for peak load demands in conventional power plants or to drive auxiliaries in other power plants, but they can also be used as base load plants in areas where fuel is cheap and readily available, and the load factor is low.

1.1.1 Aero-engines

Although gas turbine engines have land and marine applications too, but their most popular application is as aero-engines. The thrust generated by exhaust gases is used for aircraft propulsion. The Germans used gas turbine engines for aircraft propulsion for the first time in the Second World War but their use as aero-engines has evolved and become widespread ever since, owing to their qualities of compact build and high power-to-weight ratio. Today, gas turbine engines are the prime propulsive agency for aircrafts ranging from small Short Take-off and Landing to huge commercial aircrafts. Owing to the importance of these engines, constant research efforts have been going on for decades to improve their efficiency and power-to-weight ratio by making their individual components more size efficient.

1.1.2 Components of an Aero-engine and the Low-Pressure Turbine (LPT)

Most of the modern aero-engines are based on a twin spool structure in which both the compressor and turbine stages are categorized into low pressure and high-pressure stages. The mechanical power from the high-pressure turbine drives the high-pressure compressor and the low-

pressure turbine drives the low-pressure compressor. Moreover, the low-pressure turbine (LPT) is also responsible for powering the fan in turbofan engines and the propeller in turboprop engines (where it is usually called as the power turbine). Therefore, the capacity and efficiency of a low-pressure turbine play a vital role in the overall capacity and efficiency of the engine.

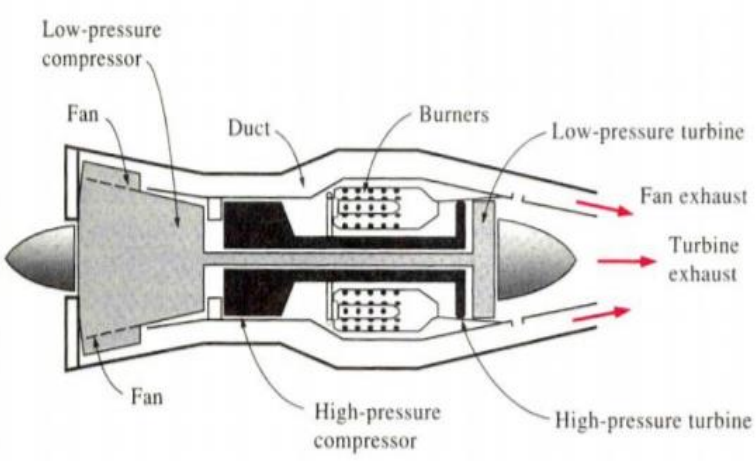

Figure 1.1: A turbofan engine with a twin spool design

The major concern with a low-pressure turbine is that it is very massive, which is for two reasons. Firstly, since the low-pressure turbine stage is responsible for extracting energy remnants from gas that has already expanded across the high-pressure stage, its size is bigger. Secondly, the LPT is made bigger to cater for the power demands of the fan and the low-pressure compressor. Usually, the LPT occupies almost one-third of the total weight of an aero-engine [1] and reducing its mass is a major research goal to increase the engine's power-to-weight ratio.

1.1.3 High Lifting Blades and Vibrations

The LPT weight can be reduced by several ways such as reducing the disk mass and the number of blades, but these can reduce the power output from the LPT. This power reduction can be compensated for by modifying the LPT blade profile. For this purpose, the blade camber is increased which enables the blades to extract more energy from the gas flow across them by creating a higher-pressure difference between the two blade sides and turning the flow by a greater angle. The blades with increased camber are called high lift blades since they generate a higher lift. Thus, high lift blades extract more energy from the expanded gas which can allow for the

reduction in disk mass and the number of blades without a reduction in power output from the LPT.

With the ultimate goal of increasing the engine power-to-weight ratio in mind, the use of high lift blades can prove to be very beneficial. But the drawback of high lift blades is that they are more prone to vibrations because of high pressure difference between the pressure and suction sides, flow separation on the suction side and increased vortex shedding. More vibrations mean increased blade flutter and more fatigue leading to increased chances of earlier failure which needs to be avoided. Chances of failure due to vibration can be reduced by applying local structural modifications such as employing lumped stiffeners, or by selecting the right blade material to increase the blade stiffness.

1.2 Blade Material

The suitability criteria for an LPT blade material are high stiffness, high natural frequency and low mass. An LPT blade of a stiffer material will have a high fundamental frequency preventing it from resonating at lower excitation frequencies, which means reduced fatigue. Using a lighter material will also have the added advantage of reducing the LPT weight. This research project is focused at comparing different materials for their stiffness, natural frequency and mass, and selecting the most suitable material for a high lifting LPT blade, based on these criteria.

1.2.1 Nickel Alloys

Nickel alloys have been widely used in turbomachinery applications due to their high strength, creep and fatigue resistance. The operating temperatures in turbines are as high as 650-1200 ^{o}C [2]. For this reason, Ni-based alloys have been very effective for use in high temperature applications particularly in the combustor stage and high-pressure turbine stage.

1.2.2 Titanium Alloys

Although Nickel based alloys were suitable enough as materials for gas turbine engine components based on their good mechanical properties, their high density of 8-8.5 g/cm^3 was seen as an issue to be addressed. This is because a larger engine weight restricts the payload weight that can be carried by the aircraft. For this reason, efforts to develop candidate materials with lower densities for aero-engine components started in the late 1970's and continued into the 80's. In this

quest for new aero-engine materials, Ti-Al alloys received the greatest amount of attention because of their lower density 4-7 g/cm^3 and potentially suitable mechanical properties [2].

Research in this field continued through the next two to three decades before the third generation Ti-Al alloys were developed. With the wide range of operating temperatures (room temperature to 850 ^{o}C), suitable mechanical properties and considerably lower density, these alloys became good candidates to replace Nickel based alloys in various aero-engine components including the LPT disk and blades [2].

This research will involve the calculation and comparison of the modal parameters of the LPT blade for these materials, and the selection of the most suitable material. The modal parameters will be calculated by computational modal analysis.

1.3 Modal Analysis

Modal analysis involves the study of dynamic response of a system in frequency domain. The inherent dynamic properties of any vibrating system also known as its 'modal parameters', include its natural frequency, mode shapes, damping ratio and remaining modal parameters (modal mass, modal stiffness and modal damping). Once we have obtained these parameters, the dynamic response of a system can be improved by performing local structural modifications.

1.3.1 Governing Equation

To understand this phenomenon, let's consider the governing equation that has been derived by S.S Rao [3]. For any system undergoing vibrations, the equation of motion can be written as,

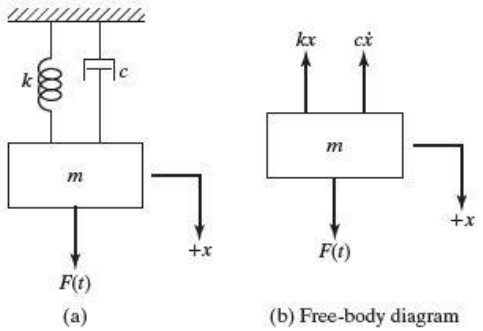

Figure 1.2: SDOF mass spring damper system [3]

$$[m]\overrightarrow{\{\ddot{x}\}} + [c]\overrightarrow{\{\dot{x}\}} + [k]\overrightarrow{\{x\}} = \overrightarrow{\{f(t)\}} \quad (1)$$

Here, m is the mass of a single degree of freedom (SDOF) system, k is its stiffness and c is the viscous damping. In our work, we shall focus on determining the inherent dynamic behavior of the LPT blade in the absence of any external excitation. Furthermore, the LPT blade is not under any viscous damping and hence the equation of motion for our analysis reduces to.

$$[m]\overrightarrow{\{\ddot{x}\}} + [k]\overrightarrow{\{x\}} = \overrightarrow{\{0\}} \quad (2)$$

In equation (I), $f(t)$ is the external exciting force. This external force is present in cased of forced vibrations while in free vibrations, the right-hand side of the equation becomes zero. The solution to the above ordinary differential equation comprises of two parts i.e., steady state solution $x_p(t)$ and the transient solution $x_h(t)$. Note that in transient response, the system is left to vibrate freely without any forcing condition and it comes to rest after a certain time. The system's overall response x(t) for (I) is obtained by superimposing both the solutions as shown in figure 1.3.

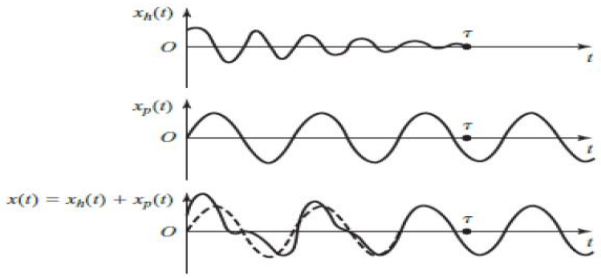

Figure 1.3: Response of a vibrating system under free vibrations

1.3.2 Frequency Domain Analysis

This response x(t) is a function of time. We can obtain this response in frequency domain $x(\omega)$ by applying a fast fourier transform (FFT) on time domain data. The frequency response data under a harmonic force generates frequency response function (FRF) plots. Each peak in an FRF plot represents a particular mode with a natural frequency, mode shape, modal mass, modal stiffness, modal damping and damping ratio. These are termed as the modal parameters. These modal parameters can be determined from FRF plots using analytical relations that will be explained later in this report.

1.3.3 Theoretical Modal Analysis

In our work, theoretical modal analysis was performed using Euler-Bernoulli beam theory. For this purpose, the LPT blade was assumed as a continuous system with a fixed-free boundary condition. The theoretically obtained values are used to validate the computational results.

1.3.4 Computational Modal Analysis

Computationally, modal analysis was performed on ANSYS 'Modal' module. The blade geometry was imported into the workbench and a fixed support was applied at its one end. The mesh independency study was performed to ascertain the most appropriate mesh sizing that yields considerably accurate results through better management of computational power.

The analysis can be performed for any number of modes or DOF (Degrees of freedom). It yields the values of natural frequencies and the corresponding mode shapes. Once the natural frequencies are obtained, they should be validated with the theoretical results obtained using the Euler Bernoulli beam theory. This validates that our computation is consistent with the mathematical model and our results are acceptable.

1.3.5 Modal Parameters

The modal parameters are the quantities that have been determined as a result of modal analysis and which completely describe dynamic behavior of a vibrating system. These quantities include the natural frequency, mode shape, damping ratio, modal mass, modal stiffness and modal damping. We will obtain the modal parameters once the choice for the most suitable blade material has been made.

The significance of this information is that it tells us at what frequencies our structure is highly likely to oscillate and what will be its corresponding mode shape at that particular frequency. Furthermore, it also helps us to model a continuous vibrating system into a discrete mass spring system with finite degrees of freedom (DOF). This helps us to locally modify a structure by adding/removing lumped masses, stiffeners thereby improve its dynamic behavior.

To determine the modal parameters, harmonic response analysis of the blade is carried out to obtain the frequency response plots. This is carried out in ANSYS where the blade is given a

fixed support and a unit force is applied at one of its ends over a wide frequency range. Each peak of the plot corresponds to a particular mode. We can determine the damping ratio at each peak by employing the half power method. With damping ratio determined, the remaining modal parameters can then be determined with the help of analytical relations.

1.4 Problem Statement

After laying a premise of all the important concepts in our work, we are now in a position to formulate our problem statement. The areas of our interest are listed as follows:

- **Mass:** The LPT (low-pressure turbine) stage of a gas turbine engine is quite massive and occupies 33% of the engine weight. The weight of the LPT stage needs to be lowered. Using high-lift blade profiles can help us reduce the weight, but it has its own drawbacks.
- **Blade Vibrations:** Vibrations are produced in the low-pressure turbine blade owing to its high lift profile. These vibrations can accelerate the fatigue-related failure of the blade.
- **Material:** Since it is not feasible to perform structural modifications, it is desired that a suitable material should be selected which not only results in reduced vibrations, but also has a low mass.

1.5 Objectives

With the areas if interest identified, let us formulate our objectives as a part of the solution to our problem statement.

- **Computational modal analysis:** To counter the problem of vibrations, we shall perform computational modal analysis of a high lift LPT blade and study its natural response using a wide range of materials.
- **Material selection:** The obtained data of natural frequency, mass and stiffness shall be compared and the most suitable material shall be chosen that has the ideal vibrational response (high frequency and stiffness) and a low mass at the same time.
- **Modal parameters:** Once the material has been selected, we shall perform an additional step by calculating its modal parameters to get a discretized mathematical model of our system under vibration.

CHAPTER 2: LITERATURE REVEW

2.1 Boundary Layer Separation and Vibrations

The high lifting low pressure turbine blades are more prone to vibrations because of the high-pressure difference between the pressure and suction sides, boundary layer separation at the rear suction side and increased vortex shedding. Rory Stieger in his PhD dissertation in Cambridge University Department of Engineering [1] and in his research on transition mechanism of highly-loaded LP turbine blades [4], has studied the effect of wake interactions on boundary layer separation of a high lift blade model. We learn from his work that modern LP turbine blades (the high lift blades) have greater boundary layer separation at the rear suction side, especially as the Reynolds number decreases. Stieger has explained the use of calm and turbulent flow to periodically suppress this boundary layer separation. According to Stieger, this new understanding of flow past a high lift blade has opened up new doors for experimental work in this direction, which will eventually make the use of high lift LP turbine blades very common. The benefits of using high lift blade profiles for LP turbine blades are that they can reportedly reduce the number of LP turbine blades by 20% thereby reducing weight and manufacturing cost without any reduction in efficiency [4].

Stieger's work confirms that a high lift blade experiences greater boundary layer separation at the suction side, and therefore is more prone to vibrations. Thus, selecting a stiffer blade material to prevent the blade from resonating at lower excitation frequencies becomes essential. The high lift blade that Stieger used in his research was a T106 blade profile.

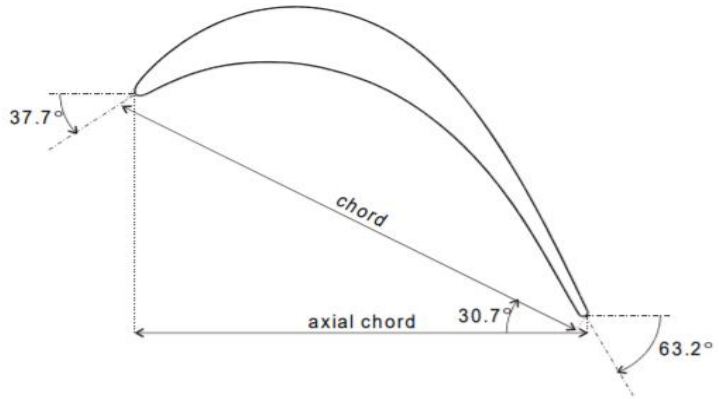

Figure 2.1: T106 LP turbine blade [1]

This research will also calculate and compare the modal parameters of the same blade profile i.e., the T106 profile using different materials, and the most suitable material will be selected.

2.2 Euler Bernoulli Beam Theory

Euler Bernoulli beam theory has been used to estimate the natural frequencies of the LPT blade that is given a fixed free boundary condition. In mechanics, Euler Bernoulli beam theory relates beam deflection against the load being applied. S.S Rao [3] in his book Mechanical Vibrations, 6th edition has derived the relation to estimate the natural frequencies of a cantilevered beam using this theory.

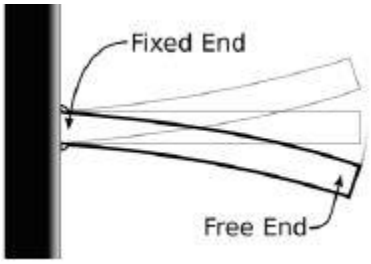

Figure 2.2: Cantilever beam in [3]

The mathematical formulation as obtained in [3] is given as,

$$\omega_n = (\beta_n l)^2 \sqrt{\frac{EI}{\rho A l^4}} \text{ (rad/s)} \tag{3}$$

Where the values of $\beta_n l$ for fixed-free condition are given below:

$\beta_1 l$=1.875104

$\beta_2 l$=4.694091

$\beta_3 l$= 7.854757

In equation (3), E is elastic modulus of the material, while ρ is its density. A, l and I are the cross-section area, length and area moment inertia of the cantilever beam.

This beam theory assumes negligible shear deformation of beam cross sections. Furthermore, it applies to a continuous domain over which it determines the natural frequencies of the system. In finite element method, the domain is discretized into a finite number of elements and the individual stiffness matrices are obtained. These results are then assembled for the entire domain. The discretization error associated with FEA can cause the results to deviate from theory. Hence, one of the challenges of our work was to ensure that the results obtained using finite element method were in substantial agreement with the results obtained using Euler Bernoulli beam theory which assumed a continuous system.

In this regard, Ali Demirtas [5] has performed the modal analysis of an aircraft wing given a fixed-free boundary condition. In his work, the computational results were validated using Euler Bernoulli beam theory. The error percentage was the least for the first mode and gradually increased for higher modes.

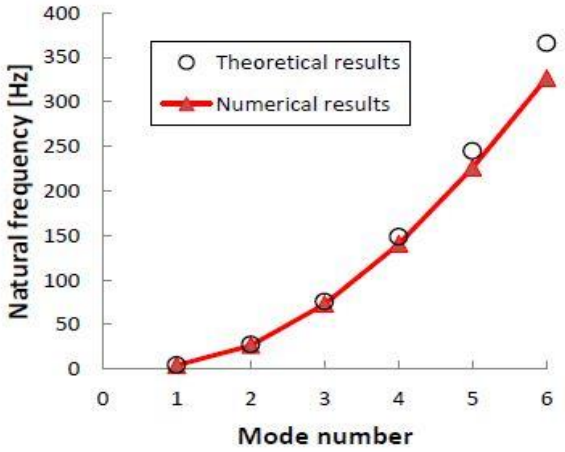

Figure 2.3: Comparison of natural frequencies of cantilever beam in [5]

2.3 Modal Analysis Techniques

Various works have been carried out to perform modal analysis either experimentally or computationally. The ultimate outcome is to determine the structure's natural frequencies, mode shapes and the remaining modal parameters so that design modifications can be made to improve the vibrational response.

In experimental modal analysis (EMA), the structure is set to oscillate with the help of a mechanical exciter or a shaker. Sensors such as accelerometers can be used to record the

displacements in time domain. The data after being processed is converted into frequency domain by applying a Fast Fourier Transform (FFT). J.K Sharma in his research work [6] has performed the experimental modal analysis of a beam under various boundary conditions. An impact hammer was used to oscillate the beam in free-free and simply supported boundary conditions. A laser vibrometer was used to measure the displacements of the beam as a function of time. A frequency response function (FRF) plot was obtained from this data and the first three modes were identified along with their frequencies. The experimental results showed a great deal of agreement with theory.

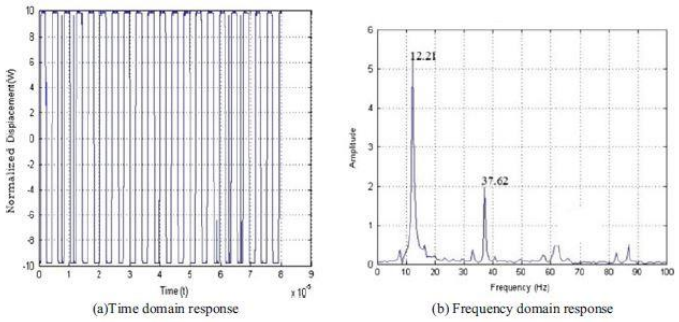

(a)Time domain response (b) Frequency domain response

Figure 2.4: Response of an S-S beam using EMA in J. K. Sharma's work [6]

Another demonstration of computational and experimental modal analysis was performed in A. R. Sonawane and P. S. Talmale's research work [7]. In this work, a cantilever beam was subjected to an impact hammer with an accelerometer placed at its free end. The data for free vibrations was recorded and analyzed. In addition, the FEA model of the cantilever beam was solved on ABAQUS. The FEA and the EMA results were further verified from theory and showed consistency.

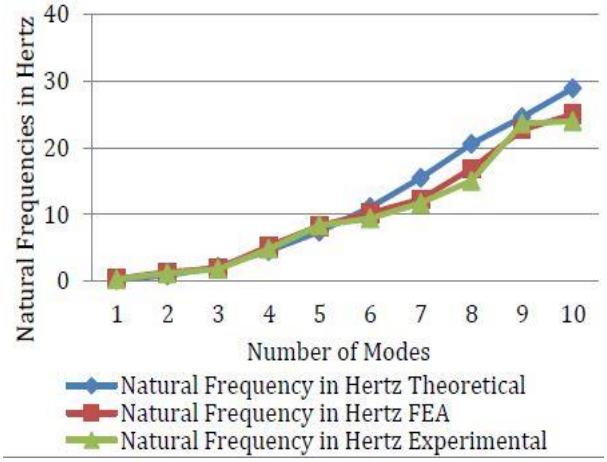

Figure 2.5: Comparison of natural frequencies for first 10 modes in A. R. Sonawane's work [7]

2.4 Comparative Study for Material Selection

Anieken Ikpe [8] has done a comparative study among two Ni-based alloys for selection as the most preferred material in a gas turbine. In his work, he has performed finite element analysis of a turbine blade that was operational at Trans Amadi Power Plant, Nigeria.

The turbine blade had a NACA6409 9% airfoil with a span of 120 mm. The analysis was performed for two Nickel based alloys i.e., IN-738 and U-500. It was observed that the materials whose natural frequency was greater than the operational frequency exhibited a longer service life. This is because due to the natural frequency being higher than the operational frequency, the chances of resonance are minimized for the blade. As a result, the blade's fatigue is reduced and the chances of failure minimized. Therefore, it is established that any modification performed in the structure is done with the aim of maximizing its natural frequency to reduce fatigue failure. Furthermore, natural frequency is structure's inherent characteristic which can be altered by modifying the design or changing the material.

In Ikpe's work [8], natural frequencies were obtained for both IN-738 and U-500 using computational modal analysis in ANSYS. The first six natural frequencies were evaluated for each. U-500 possessed a higher fundamental frequency (896 Hz) as compared to IN-738 (751 Hz). Hence, it was established that U-500 was a suitable blade material for higher stages of a turbine blade as it possessed a greater fundamental frequency.

This study shall be used as a guideline for us in this work during the process of selecting the most suitable blade material. In addition, we shall also consider the stiffness and mass of the blade in addition to its natural frequency while making the suitable blade material choice.

2.5 Materials for Gas Turbine Engines

2.5.1 Nickel Based Alloys

With the developments and advancements in gas turbine technology, it has been established that for improved efficiency of a gas turbine, the turbine entry temperature (TET) has to be kept to a maximum [9]. For this reason, efforts have been made to develop materials that possessed significant creep resistance at high temperatures (as high as 1200 ^{o}C in turbine). Co and Ni based

alloys were chosen primarily for use in turbine stages and combustor. Later on, Co based alloys were replaced completely with Ni-based due to natural abundance of Ni in earth's crust. Typically, 47% of an aircraft engine is composed of Nickel alloys due to its high strength applications and endurance at elevated temperatures [9].

Nageswara Rao has listed the compositions and applications of various Nickel alloys in his work [2]. According to his work, combustor stage where temperatures are high, Hastelloy, Nimonic and Haynes classes of Ni-alloys are used since they contain a higher percentage of Cr which enhances the corrosion resistance of the alloy. For turbine stages, high fatigue and creep strength is also needed in addition to corrosion resistance. Therefore, for turbine stages, Udimet and Inconel are mostly used as they contain significantly higher percentage of Ti and Al which improve the strength/weight ratio for blading applications.

2.5.2 Ti-Al Based Alloys

Major aero-engine manufacturing companies and researchers have been trying to develop light weight alloys to replace the heavier Nickel based alloys in various aero-engine components. These efforts started back in the 1970's and continued through the decades to follow. In this search for alternatives, Ti-Al based alloys have shown the most compelling properties. With significantly lower densities compared to most Nickel based alloys (4-7 g/cm^3 compared to 8-8.5 g/cm^3 of Nickel based alloys), the Ti-Al based alloys show almost similar mechanical properties. Furthermore, advanced Ti-Al based alloys can operate in wide temperature ranges which makes them ideal candidates to replace Nickel based alloys in aero-engines [2].

The blades of a low-pressure turbine operate in extreme conditions of high temperature and pressure. These conditions demand the blades to be of strong materials. Not only Ti-Al based alloys fulfil the strength criteria, but the high Aluminum content makes them resistant to corrosion and oxidation- making these alloys adequately suitable candidates for working in these conditions.

Besides the advantages of reduced mass of blades, the use of Ti-Al alloys can help in reducing the weight of other aero-engine components too. Previously, the turbine disks and spools were made from massive Nickel based alloys to counter the high centrifugal forces acting on them. The use of Ti-Al alloys reduces the centrifugal forces allowing for weight reduction modifications

for the disks and spools. In this way, the engine weight can be reduced to enhance fuel efficiency and reduce carbon dioxide emissions.

The major obstacle that stood in the way of using Ti-Al alloys in aero-engines was the difficulty to form these using conventional and affordable forming techniques because of their poor ductility [10]. Also, these alloys showed very low tolerance to manufacturing defects making their manufacturing very difficult and expensive [11]. For these reasons, most of the latest research in the field of Ti-Al alloys is focused on finding ways to make their manufacturing easier and more efficient. In this regard, newer manufacturing techniques such as additive manufacturing, electron beam melting technology and laser powder bed fusion technology have shown encouraging results [11].

CHAPTER 3:METHODOLOGY

In this research, materials for a high lift LP turbine blade are to be compared on the criteria of high natural frequency, high stiffness and low mass. Therefore, to compare the materials under study, these parameters are to be calculated for the blade using each material. Since natural frequency is an inherent dynamic property of the blade, it can be calculated by performing modal analysis. Modal analysis can be performed theoretically, computationally and experimentally. The approach that will be used in this research is that the modal parameters of the blade will be calculated by computational modal analysis and the results will be verified by comparison with results obtained from theory.

To validate this approach, the procedure will be first performed on a cantilever beam with a rectangular cross section, before performing for the actual blade model. The beam geometry has been taken from the research work of S. P. Chaphalkar, Subhash. N. Khetre and Arun. M. Meshram [12], who have performed the modal analysis of a cantilever beam using experimental and FEA methods. The cantilever beam's transverse natural frequencies will be calculated from theory and computation and the two results will be compared. To further verify the approach, the results will also be compared to experimental results from Chaphalkar's work [12], and the credibility of the approach will be judged based on the percentage error between the results from different methods.

3.1 Modal Analysis of the Cantilever Beam

In this section, modal analysis of the cantilever beam will be performed using theoretical and computational methods.

3.1.1 Theoretical Modal Analysis

Theoretically, the natural frequencies of a beam in the transverse bending direction can be calculated by using Euler Bernoulli beam theory. This theory provides different relations that can be used to calculate the natural frequencies of beams with different boundary conditions, such as fixed-free, free-free, and simply supported beams. Since an LP turbine blade is fixed at one end and free at the other, it behaves as a fixed-free/cantilever beam. For this reason, we are performing the analysis first on a simple cantilever beam with a rectangular cross section.

From Euler Bernoulli beam theory, the natural frequencies of a cantilever beam in the transverse bending direction can be calculated by using the following relation [3]:

$$\omega_n = (\beta_n l)^2 \sqrt{\frac{EI}{\rho A l^4}} \text{ (rad/s)}$$

For natural frequency in Hertz:

$$f_n = \frac{(\beta_n l)^2}{2\pi} \sqrt{\frac{EI}{\rho A l^4}} \ (Hz) \tag{4}$$

In this relation, E is the material's elastic modulous, ρ is the material's density, I,A and l are the moment of inertia, area of cross section and length of the beam, respectively. 'n' stands for the number of mode, and the quanity '$\beta_n l$' is a constant for each mode. For the first three modes, i.e., n=1,2 & 3:

$\beta_1 l$=1.875104

$\beta_2 l$=4.694091

$\beta_3 l$= 7.854757

The cantilever beam's properties from [12] are:

Length (l) = 0.8m

Width (b) = 0.05m

Height (h) = 0.006m

Beam material : Mild Steel

Young's modulous (E) = 210 GPa

Density (ρ) = 7856 kg/m^3

Poisson ratio = 0.3

First of all, the beam's moment of inertia is calculated using the relation:

$$I = \frac{1}{12} b h^3 \tag{5}$$

So,

$$I = \frac{1}{12}(0.05)(0.006)^3$$

This gives,

$$I = 9 \times 10^{-10}\ m^4$$

The next step is putting values in (4) to calculate the natural frequencies:

- For mode 1:

$$f_1 = \frac{(\beta_1 l)^2}{2\pi}\sqrt{\frac{EI}{\rho A l^4}}$$

$$f_1 = \frac{(1.875104)^2}{2\pi}\sqrt{\frac{(210 \times 10^9)(9 \times 10^{-10})}{(7856)(0.05 \times 0.006)(0.8)^4}}$$

This gives,

$$f_1 = 7.83\ Hz$$

- For mode 2:

$$f_2 = \frac{(\beta_2 l)^2}{2\pi}\sqrt{\frac{EI}{\rho A l^4}}$$

$$f_2 = \frac{(4.694091)^2}{2\pi}\sqrt{\frac{(210 \times 10^9)(9 \times 10^{-10})}{(7856)(0.05 \times 0.006)(0.8)^4}}$$

This gives,

$$f_2 = 49.06638\ Hz$$

- For mode 3:

$$f_3 = \frac{(\beta_3 l)^2}{2\pi}\sqrt{\frac{EI}{\rho A l^4}}$$

$$f_3 = \frac{(7.854757)^2}{2\pi}\sqrt{\frac{(210 \times 10^9)(9 \times 10^{-10})}{(7856)(0.05 \times 0.006)(0.8)^4}}$$

This gives,

$$f_3 = 137.3873\ Hz$$

With the first three transverse natural frequencies calculated from theory, the next step is to calculate the same by computational modal analysis.

3.1.2 Computational Modal Analysis

Computational modal analysis of the cantilever beam was performed in ANSYS 'Modal' module. This module is used to study free vibrations of structures. In computational/numerical procedure, the physical structure is converted into a mathematical model using some assumptions. The assumptions generate differential equations that govern the mathematical model.

To start the procedure, the beam geometry was imported to ANSYS Modal and Mild Steel material was assigned to it, and mesh was generated.

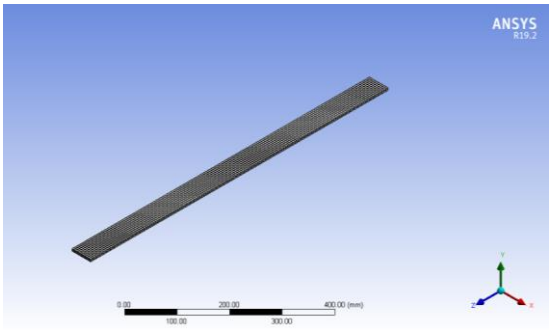

Figure 3.1: Cantilever beam with mesh in ANSYS Mechanical

In computational Finite Element Analysis, the entire structure is divided into smaller elements by applying mesh. Since FEA is a numerical technique that uses assumptions, the solution accuracy becomes a major concern. Generally, the solution accuracy increases by mesh refinement, but the solution then requires more computational power and time. This issue can be solved by performing mesh independency analysis to select an optimum mesh size. Mesh independency analysis basically provides the mesh size after which making the mesh finer does

not significantly affect the solution accuracy. In other words, the results become mesh independent. The mesh independency graph is given in figure 3.2.

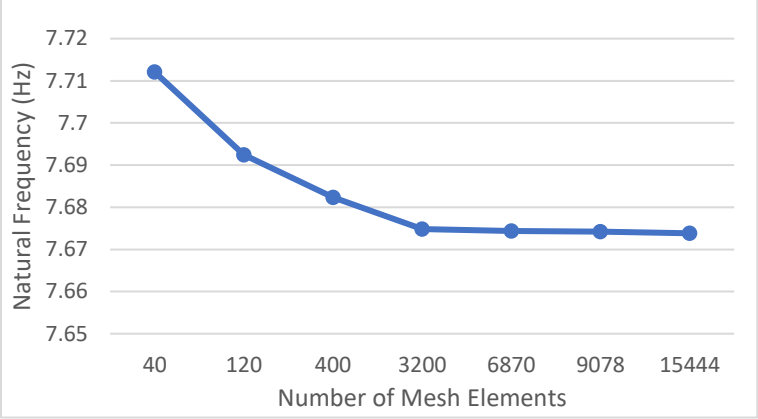

Figure 3.2: Mesh independency graph

From this graph, it can be seen that after 3200 elements, there is no significant change in frequency as the number of elements is increased. Thus, mesh independency was achieved at 3200 mesh elements and the corresponding element size i.e., 5mm was selected.

After mesh generation, analysis settings were applied. Fixed-support boundary condition was applied at one end of the beam, while the other end was left free.

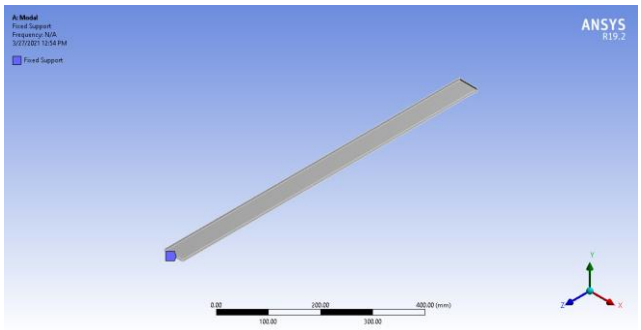

Figure 3.3: Fixed-free boundary condition applied in analysis settings

The system was solved for the first 6 transverse bending modes to generate the corresponding natural frequencies and mode shapes. Of the first 6 modes, mode numbers 1, 2 and 4 were the first three modes in the transverse direction. The natural frequencies for these modes from ANSYS are:

- For mode 1:

$$f_1 = 7.6748\ Hz$$

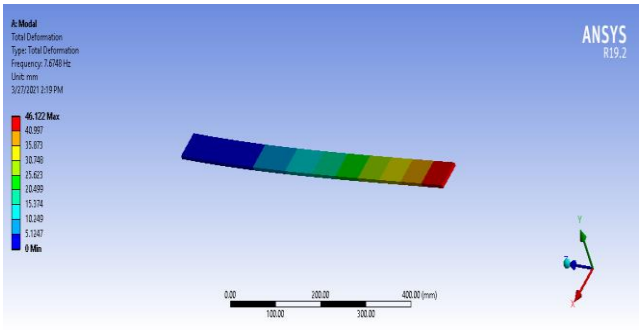

Figure 3.4: Mode shape for first mode

- For mode 2:

$$f_2 = 48.081\ Hz$$

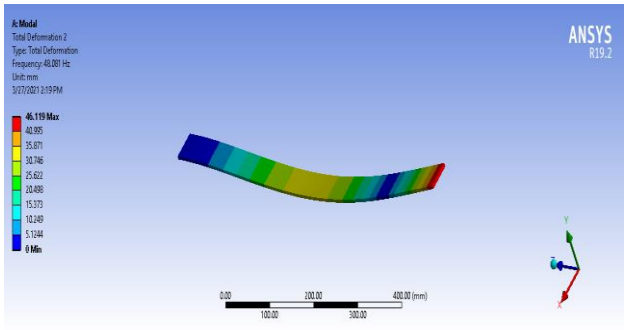

Figure 3.5: Mode shape for second mode

- For mode 3:

$$f_3 = 134.61\ Hz$$

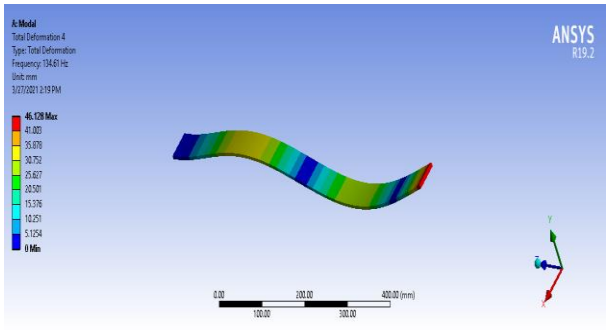

Figure 3.6: Mode shape for third mode

With the first three transverse natural frequencies obtained from computation, the next step is to look at the values obtained from experimental modal analysis of the beam.

3.1.3 Experimental Modal Analysis

The cantilever beam's natural frequencies from experimental modal analysis were obtained from Chaphalkar's work [12]. For experimental modal analysis, the beam was fixed at one end, and the other end was left free. An accelerometer was mounted at the free end, and this end was given an initial displacement. After the initial displacement, the beam was left to vibrate freely.

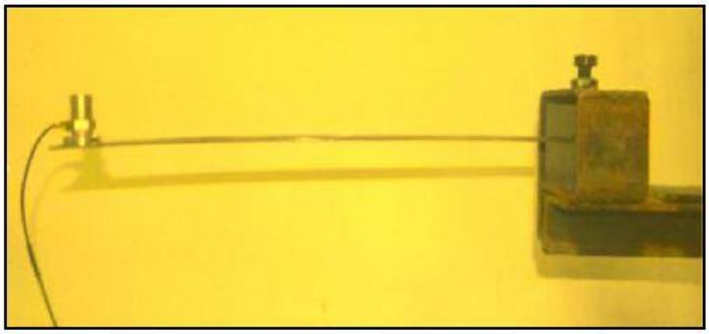

Figure 3.7: Experimental setup of a fixed free beam with an accelerometer mounted at the free end [12]

Time domain data from the transducer was converted to frequency domain and recorded. Frequencies for the first three transverse modes obtained from this method are:

- For mode 1:

$$f_1 = 7.6769\ Hz$$

- For mode 2:

$$f_2 = 48.1001\ Hz$$

- For mode 3:

$$f_3 = 134.6906\ Hz$$

3.1.4 Comparison of Results

After obtaining the cantilever beam's transverse natural frequencies by theoretical, computational and experimental methods, the next step is to compare these results. After comparison of results, it will be possible to assess if this approach is valid or not.

Table 3.1: Comparison of theoretical, computational and experimental natural frequencies of a cantilever beam

Mode Number	Theoretical Natural Frequency (Hz)	Computational Natural Frequency (Hz)	Experimental Natural Frequency (Hz)	% Error (theory and computation)	% Error (theory and experiment)
1	7.83	7.6748	7.6769	1.9821	1.95530
2	49.06638	48.081	48.1001	2.0082	1.96933
3	137.3873	134.61	134.6906	2.0215	1.96284

It can be seen from the table that the values of natural frequency obtained from the three methods are in close agreement with each other. The values obtained through computation and experimentation are slightly different than the exact values from theory because of measurement errors that happen in experimentation and assumptions that are used in FEA. Nevertheless, the percentage error between theory and computation, and theory and experimentation are quite small, which validates the approach. The same can be seen in figure 3.8.

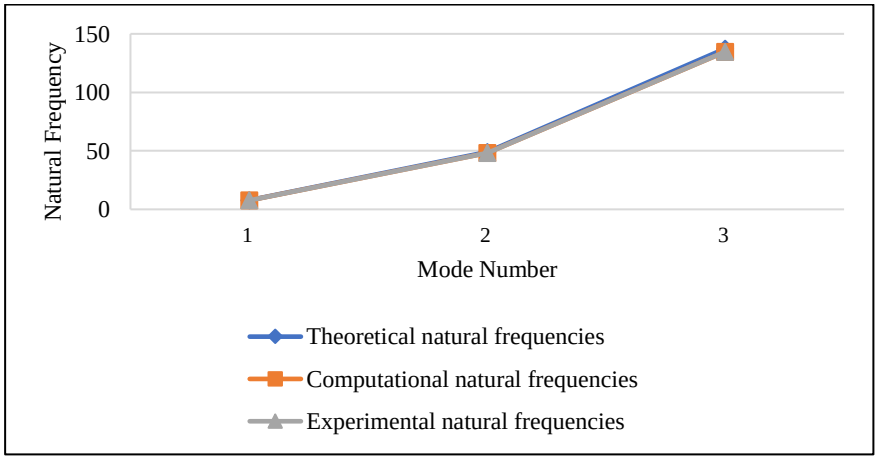

Figure 3.8: Comparison of theoretical, computational and experimental natural frequencies of a cantilever beam

From this study, it can be concluded that this approach is valid. Therefore, the same approach will be used for the analysis of the actual high lift LP turbine blade model (T106). Modal parameters will be calculated from computation and verified by comparison with results obtained from theory.

3.2 Modal Analysis of T106 Blade

With the modal analysis methodology validated from the cantilever beam example, the same procedure will be performed for the T106 blade. The blade natural frequencies for the first two transverse bending modes will be calculated from theory and computation for all materials under study, and the results from computation will be compared with the theoretical results for validation.

3.3 Blade Materials for Modal Analysis

- **Nickel Based Alloys**

Table 3.2: List of Ni-based alloys along with compositions

S#	Alloy	Composition
1	U-500	18Cr-10Co-4.2Mo-3Al-3Ti-0.07C-0.007B-0.05Zr
2	IN-738	16Cr-8.5Co-1.75Mo-2.6W-1.75Ta-0.9Nb-3.4Ti-3.4Al-0.04Zr-0.11C-0.01B
3	MAR-M246	9Cr-10Co-2.5Mo-10W-1.5Ta-5.5Al-1.5Ti-0.14C-0.015B-0.05Zr
4	PWA-1480	10Cr-5Co-4W-12Ta-5Al-1.5Ti
5	IN-713	12Cr-4.5Mo-5.9Al-0.6Ti-0.05C-0.01B-0.1Zr-2Nb
6	IN-100	10Cr-15Co-3Mo-5.5Al-4.7Ti-0.18C-0.014B-0.06Zr-1V
7	Rene' N4	9Cr-8Co-2Mo-6W-4Ta-0.5Nb-3.7Al-4.2Ti
8	Rene' N5	63.1Ni-7Cr-7.5Co-1.5Mo-5W-3Re-6.5Ta-0.15Hf-6.2Al-0.05C-0.004B-0.01Y
9	CMSX-2	8Cr-5Co-0.6Mo-8W-6Ta-5.6Al-1Ti-0.1Hf
10	CMSX-4	6.4Cr-9.6Co-0.6Mo-6.4W-6.5Ta-5.6Al-1Ti-0.1Hf-3Re
11	PWA-1484	5Cr-10Co-2Mo-6W-8.7Ta-5.6Al-0.1Hf-3Re
12	U-700	59Ni-14.3Cr-14.5Co-4.3Mo-3.5Ti-4.3Al-0.02Zr-0.08C-0.015B
13	SU-263	20Ni-20Cr-0.4Co-6Fe-2.1Mo-0.4Ti-0.06Al-1C
14	IN-738 LC	16Cr-8.5Co-1.7Mo-2.6W-1.7Ta-3.4Al-3.4Ti-0.1C-0.01B-0.05Zr-0.9Nb
15	Rene 41	19Cr-10.5Co-9.5Mo-3.2Ti-1.7Al-0.01Zr-0.08C-0.005B

- **Ti-Al Based Alloys**

Table 3.3: List of Ti-Al alloys along with compositions

S#	Alloy	Composition
1	Ti-64	Ti-6Al-4V
2	Ti-811	Ti-8Al-1Mo-1V
3	Ti-834	Ti-5.8Al-4Sn-3.5Zr-0.7Nb-0.5Mo-0.35Si-0.06C
4	Ti-1100	Ti-6Al-2.8Sn-4Zr-0.4Mo-0.4Si
5	Ti-6242	Ti-6Al-2Sn-4Zr-2Mo
6	Ti-685	Ti-6Al-5Zr-0.5Mo-0.25Si
7	Ti-829	Ti-5.5Al-3.5Sn-3Zr-1Nb-0.25Mo-0.3Si
8	Alpha-2	Ti-24.5Al-12.5Nb-1.5Mo
9	Ti-662	Ti-6Al-6V-2Sn
10	Ti-6246	Ti-6Al- 2Sn-4Zr-6Mo
11	Gamma-2	Ti-48Al-2Cr-2Nb
12	Ti-62s	Ti-6A1-2Fe-0. 1Si
13	Ti-5-2.5	Ti-5Al-2.5Sn
14	Ti-679	Ti-11Sn-5Zr-2.25Al-1Mo-0.25Si
15	Ti-54M	5Al-4V-0.6Mo-0.5Fe

3.4 Theoretical Modal Analysis of T106 Blade

Similar to the theoretical modal analysis of the cantilever beam, the T106 blade's first two natural frequencies in transverse direction will be calculated from Euler Bernoulli beam theory. As mentioned earlier, Euler Bernoulli theory provides relations for natural frequencies of a beam with various boundary conditions, but since an LP turbine blade is fixed at one end and free at the other, the relation for cantilever beam from equation (4) will be used:

$$f_n = \frac{(\beta_n l)^2}{2\pi}\sqrt{\frac{EI}{\rho A l^4}}\ (Hz)$$

In this equation, the quanity '$\beta_n l$' is a constant for each mode. For the first two modes, i.e., n=1 & 2:

$$\beta_1 l = 1.875104$$

$$\beta_2 l = 4.694091$$

And,

Blade span/length (l) = 0.375 m

Beam material : Nickel based alloys & Ti-Al based alloys

Young's modulous (E) is different for each material

Density (ρ) is different for each material

The cross sectional properties were determined using Solidworks as shown in figure 3.9. We were interested in the cross-section area and principal moment of intertia along x-axis at the centroid which come out to be:

Cross sectional area of the blade (A) = 0.00345 m

Blade moment of inertia (I) = 9.3×10^{-7} m^4

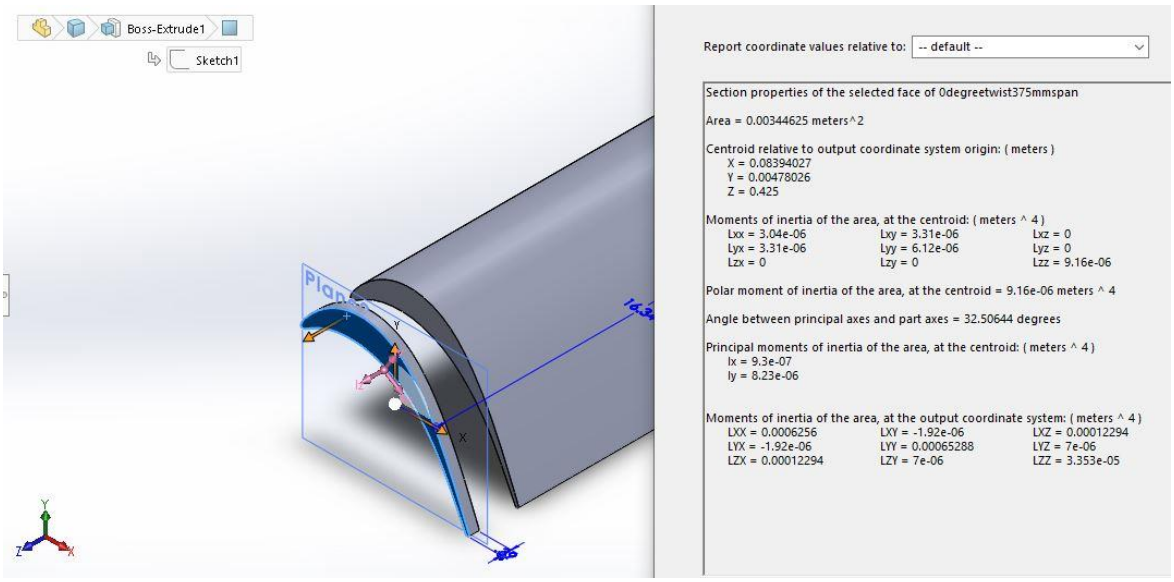

Figure 3.9: Section properties using Solidworks

3.4.1 Calculation of Natural Frequencies for Nickel Based Alloys

For the Nickel based alloy U-500:

Young's modulus (E) = 190 GPa

Density (ρ) = 7800 kg/m^3

So,

$$f_1 = \frac{(\beta_1 l)^2}{2\pi}\sqrt{\frac{EI}{\rho A l^4}}$$

$$f_1 = \frac{(1.875104)^2}{2\pi}\sqrt{\frac{(190\times10^9)(9.3\times10^{-7})}{(7800)(0.00345)(0.375)^4}}$$

This gives,

$$f_1 = 322.61\ Hz$$

&

$$f_2 = \frac{(\beta_2 l)^2}{2\pi}\sqrt{\frac{EI}{\rho A l^4}}$$

$$f_2 = \frac{(4.694091)^2}{2\pi}\sqrt{\frac{(190\times10^9)(9.3\times10^{-7})}{(7800)(0.00345)(0.375)^4}}$$

This gives,

$$f_2 = 2021.7597\ Hz$$

The same calculations were performed for the remaining fourteen Nickel based alloys. The Young's moduli, densities, and the obtained natural frequencies for all fifteen Nickel based alloys are tabulated in table 4.1 in chapter 4.

3.4.2 Calculation of Natural Frequencies for Ti-Al Based Alloys

For the Ti-Al alloy Ti-64:

Young's modulus (E) = 114 GPa

Density (ρ) = 4430 kg/m^3

So,

$$f_1 = \frac{(\beta_1 l)^2}{2\pi}\sqrt{\frac{EI}{\rho A l^4}}$$

$$f_1 = \frac{(1.875104)^2}{2\pi}\sqrt{\frac{(114\times10^9)(9.3\times10^{-7})}{(4430)(0.00345)(0.375)^4}}$$

This gives,

$$f_1 = 331.297\ Hz$$

&

$$f_2 = \frac{(\beta_2 l)^2}{2\pi}\sqrt{\frac{EI}{\rho A l^4}}$$

$$f_2 = \frac{(4.694091)^2}{2\pi}\sqrt{\frac{(114\times10^9)(9.3\times10^{-7})}{(4430)(0.00345)(0.375)^4}}$$

This gives,

$$f_2 = 2076.2005\ Hz$$

The same calculations were performed for the remaining fourteen Ti-Al based alloys. The Young's moduli, densities, and the obtained natural frequencies for all fifteen Ti-Al based alloys are tabulated in table 4.2 in chapter 4.

3.5 Computational Modal Analysis of T106 Blade

As we have obtained the natural frequency results using the analytical method, the next step is to perform the computational modal analysis on our blade geometry. Our aim will be to determine the natural vibrational response of the structure using different alloys and then choose the most ideal material amongst those. The settings of our analysis were as follows:

3.5.1 Geometry

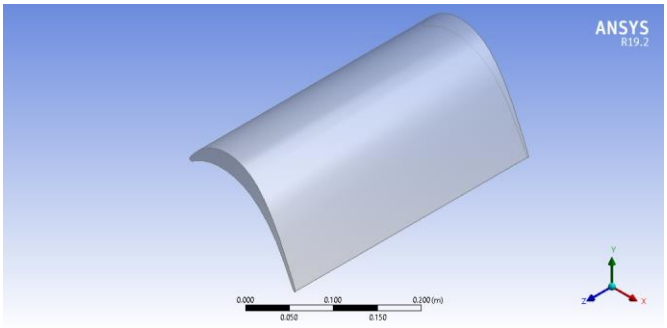

Figure 3.10: T106 blade geometry in ANSYS

The T106 blade was modelled in PTC Creo. The airfoil coordinates were obtained from [1]. The blade was modelled with a span of 375mm with 0 degrees of twist angle. The geometry was imported in Workbench in IGES format.

3.5.2 Mesh

The mesh settings had a significant impact on the accuracy of computational findings, e.g., natural frequency in particular. Therefore, it was mandatory to determine the optimal mesh sizing at which the discretization error was minimized.

A mesh independency study was performed to obtain an acceptable of results while managing our computational resources at the same time. Due to an unsymmetrical and highly cambered airfoil cross section, tetrahedral elements were chosen as compared to hexahedral element geometry. The results of second natural frequency of the blade are plotted against the number of elements in the following figures.

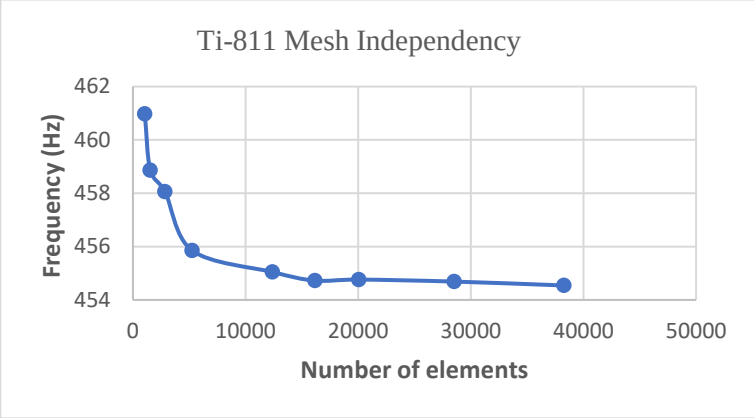

Figure 3.11: Mesh independency plot for Ti-811

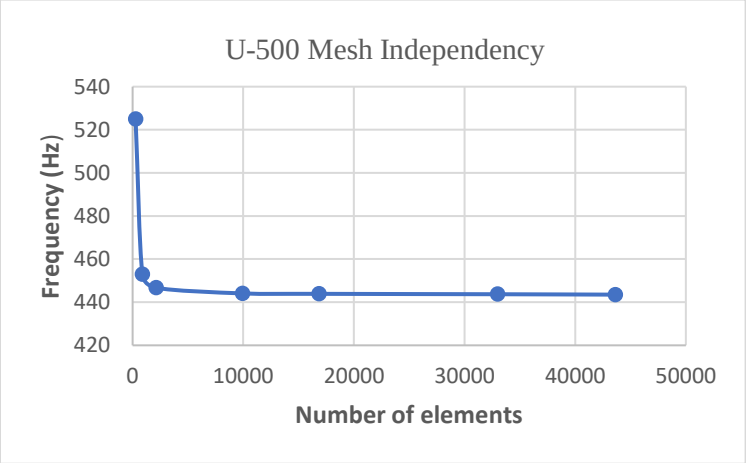

Figure 3.12: Mesh independency plot for U-500

In figures 3.11 and 3.12, plots for mesh independency have been added for a titanium-based alloy Ti-811, and a Ni-based alloy which is Udiment-500 respectively. Both these plots show a significant variation in results as the number of elements increases. The results eventually become independent on mesh at higher number of elements as the discretization error is reduced.

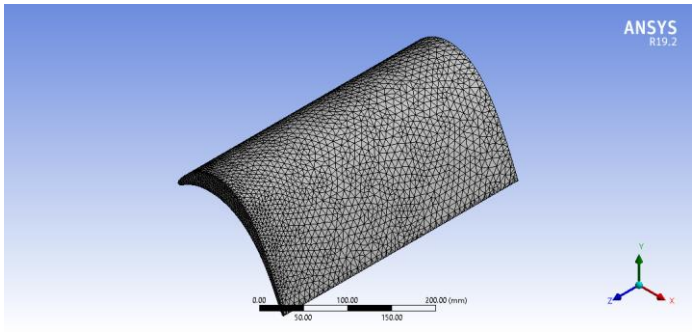

Figure 3.13: Meshing of Ti-811

However, higher element computation requires more resources and hence an optimal number of elements should be chosen. We choose the point from where the curve begins to flatten. In figure 3.11, this point falls around 16000 elements whereas in figure 3.12, the curve begins to flatten around 2000 elements.

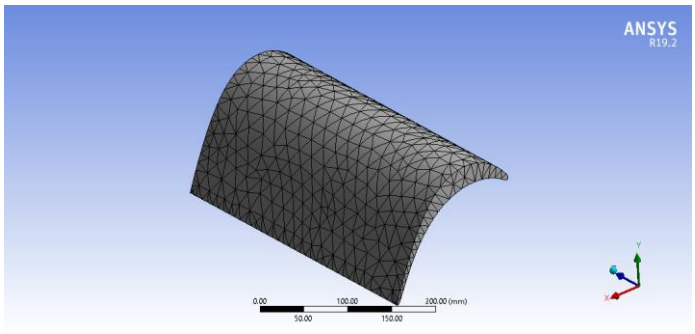

Figure 3.14: Meshing of U-500

This mesh independency study was performed on the complete set of materials including both Ni-based and Ti-based alloys. The optimal mesh setting was determined for each material as a result of this study.

3.5.3 Modal Analysis Settings

The blade in actual LPT is fixed at its one end and free at the other. Hence, to model an actual LPT blade, one end was given a fixed constraint while the other was kept free. The analysis was performed for the first 7 modes.

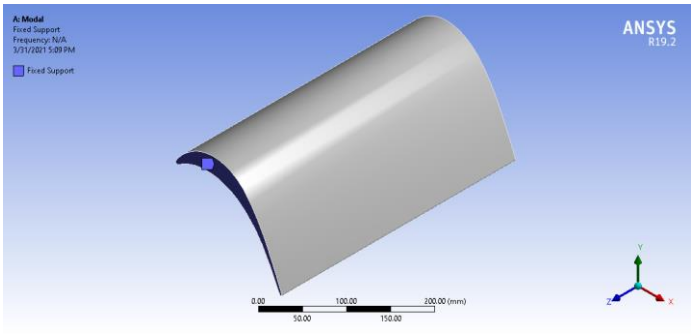

Figure 3.15: Boundary conditions in ANSYS for T106 blade

Once the choice has been made for the suitable blade material, we shall proceed towards determining its modal parameters (modal mass, modal stiffness, modal damping, and damping

ratio). The significance of these parameters is that each mode can be modelled as a SDOF mass-spring system which enables us to perform local structural modifications if an improvement in vibrational performance is desired.

3.6.1 Harmonic Analysis

To obtain these modal parameters, we need the frequency response function (FRF) of the blade. This can be performed using the "Harmonic Response" module in ANSYS. As explained in chapter 1, modal analysis deals with the transient or free vibration response of an oscillating structure. While harmonic analysis deals with the response under the action of a harmonic force.

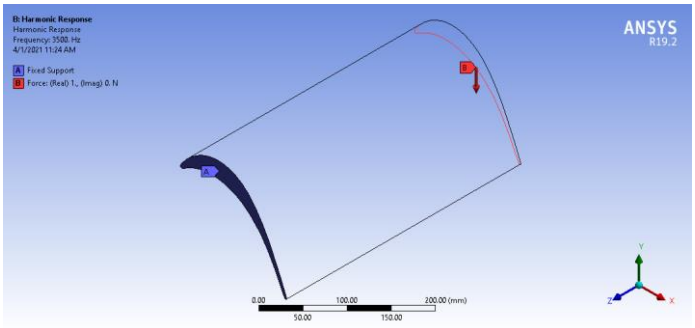

Figure 3.16: Boundary conditions during harmonic analysis

The frequency of the harmonic force also known as the excitation frequency is given a certain range. The blade's deformation at this frequency range is thus obtained as an FRF plot.

As a sample, the boundary conditions for U-500 in harmonic analysis are provided in figure 3.16. The settings used in the analysis are given in table 3.4.

Table 3.4: Harmonic analysis setting in ANSYS

Parameter	Value
Force Magnitude	1 N
Force Direction	-Y
Frequency Range	0-2000 Hz
Solution Intervals	200

3.6.2 Frequency Response Plot

A plot of displacement as a function of frequency was obtained as a result of harmonic analysis. Using the settings in table 3.4, a sample graph for displacement magnitude obtained using U500 is provided in figure 3.17.

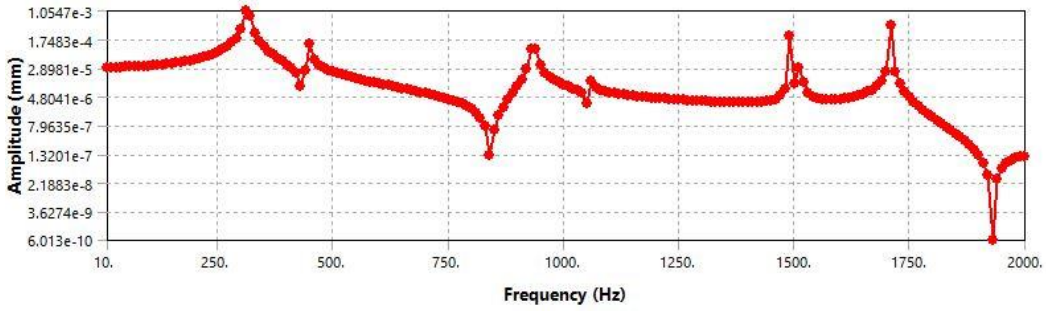

Figure 3.17: Frequency response plot for displacement (U500)

The plot in figure 3.17 conveys information about the receptance or admittance of a vibrating system. The receptance is defined as the displacement of a vibrating body per unit applied force and has units of m/N. Based on such plots, engineers can determine the resonant frequencies of a structure as each peak corresponds to such a frequency. Furthermore, we can determine the modal parameters which can help us perform local structural modifications, if needed.

3.6.3 Peak Picking Method

S.S. Rao [13] has derived a relation for obtaining the quality factor or bandwidth from a frequency response plot. The relation is provided below:

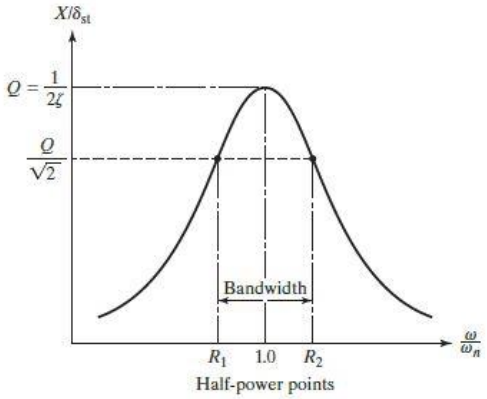

Figure 3.18: Half power points shown in harmonic response curve

$$Q = \frac{1}{2\zeta} = \frac{\omega_n}{\omega_2 - \omega_1} \tag{6}$$

ω_2 and $\omega_1$are the frequencies at half power points 2 and 1 respectively. The half power points are the values at which response becomes $\frac{1}{\sqrt{2}}$ times the peak response. ω_n is the peak or natural frequency at that particular mode. By rearranging (6), we can obtain the relation for damping ratio at a certain peak/mode.

$$\zeta = \frac{\omega_2 - \omega_1}{2\omega_n} \tag{7}$$

3.6.4 Calculation of Modal Mass, Stiffness and Damping

Richardson [14] has derived the relations for computing modal mass, stiffness and damping from experimental modal data. We shall use these mathematical relations to calculate the remaining modal parameters. These relations are provided as follows:

$$[m] = \left[\frac{1}{A\omega}\right] \tag{8}$$

$$[k] = \left[\frac{\sigma^2 + \omega^2}{A\omega}\right] \tag{9}$$

$$[c] = \left[\frac{2\sigma}{A\omega}\right] \tag{10}$$

Some basic relations are given as follows:

$$s = \sigma \pm j\omega \tag{11}$$

$$\sigma = \zeta\omega \tag{12}$$

$$A = H(\omega)\sigma \tag{13}$$

Here,

n = number of modes

[m] = (n x n) modal mass matrix

[k] = (n x n) modal stiffness matrix

[c] = (n x n) modal damping matrix

s = poles of a transfer function

A = scaling factor

ω = natural frequency

σ = real part of s

3.6.5 Curve fitting

These modal parameters can be plotted as bode plots on MATLAB using transfer function approach. Each mode represents a SDOF system and hence can be represented by a transfer function provided as:

$$H(\omega) = \frac{1}{ms^2 + cs + k} \tag{14}$$

This relation (14) is obtained by taking the Laplace transform of equation of motion (1). Using modal parameters, we can curve fit the FRF plots determined using ANSYS and the bode plots obtained from MATLAB. Curve fitting can help us determine that up to what extent the results from the transfer function approach and harmonic analysis relate with each other.

CHAPTER 4: RESULTS AND DISCUSSIONS

4.1 Analytical Results

As explained in chapter 3, the T106 blade's first two natural frequencies in the transverse bending direction were calculated using Euler Bernoulli beam theory. Sample calculations were performed for the Nickel based alloy U-500 and the Ti-Al based alloy Ti-64. Natural frequencies of the remaining alloys were calculated using the same method and the results are given below:

4.1.1 Nickel Based Alloys:

The Young's moduli, densities, and the analytically obtained natural frequencies for all fifteen Nickel based alloys are given in table 4.1.

Table 4.1: Theoretical natural frequency results for Nickel based alloys

S. No.	Alloy Name	Young's Modulus (E) (GPa)	Density (ρ) (kg/m^3)	First Natural Frequency (f_1) (Hz)	Second Natural Frequency (f_2) (Hz)
1	U-500	190	7800	322.61	2021.7597
2	U-700	186	7696.4	321.294	2013.5124
3	PWA-1484	106	8800	226.325	1418.3549
4	PWA-1480	106	8700	227.622	1426.4831
5	Rene N4	106	8400	231.651	1451.7325
6	Rene N5	106	8600	228.942	1434.7526
7	Rene 41	218	8250	336.008	2105.7233
8	CMSX-2	106	8560	229.476	1438.101
9	CMSX-4	106	8700	227.622	1426.4831
10	IN-738	149	8550	272.871	1710.0551
11	IN-713	200	7913	328.619	2059.4177
12	IN-100	215	7750	344.283	2157.5874
13	IN-738 LC	168	7892.7	301.472	1889.2944
14	MAR-M246	210	8440	326.051	2034.3297
15	SU-263	179	8130.7	306.698	1922.0407

4.1.2 Ti-Al Based Alloys:

The Young's moduli, densities, and the analytically obtained natural frequencies for all fifteen Ti-Al based alloys are given in table 4.2.

Table 4.2: Theoretical natural frequency results for Ti-Al based alloys

S. No.	Alloy Name	Young's Modulus (E) (GPa)	Density (ρ) (kg/m^3)	First Natural Frequency (f_1) (Hz)	Second Natural Frequency (f_2) (Hz)
1	Ti-64	114	4430	331.297	2076.2005
2	Ti-811	120	4370	342.529	2146.5941
3	Ti-834	120	4550	335.686	2103.7055
4	Ti-1100	120	4510	337.171	2113.014
5	Ti-6242	120	4540	336.055	2106.0211
6	Ti-685	125	4450	346.436	2171.076
7	Ti-829	120	4540	336.055	2106.0211
8	Alpha-2	145	4840	357.774	2242.1329
9	Ti-662	110	4540	321.748	2016.3617
10	Ti-6246	115	4640	325.415	2039.3415
11	Gamma-2	176	4040	431.433	2703.7447
12	Ti-62s	128	4440	350.963	2199.4471
13	Ti-5-2.5	125	4480	345.274	2163.7946
14	Ti-679	107	4840	307.338	1926.0574
15	Ti-54M	113	4650	322.226	2019.3555

These natural frequency results obtained from theory will be used to validate the results obtained from computation.

4.2 Computational Results

The 'Modal' analysis on ANSYS performed the extraction of first 7 modes and their natural frequencies. These modes comprised of bending modes in X and Y directions as well as torsional modes. The X-direction is the line join the leading edge to the trailing edge of the blade. Y-direction is from the pressure side towards the blade's suction side whereas Z-direction is along the blade length (from free end towards the fixed end).

4.2.1 Transverse Bending Modes

We are specifically interested in the bending mode along Y direction. This is because in normal operation, LPT blades undergoing vibration in the transverse bending mode are highly likely to strike with each other. This further raises the chances of blade failure particularly at such high shaft RPM. Hence, we shall obtain and compare the fundamental frequencies of each material in the transverse bending modes of the LPT blade and choose the one which displays the most

suitable response. Figure 4.1 shows the transverse bending direction of the blade. This is the first Y-mode shown for U-500.

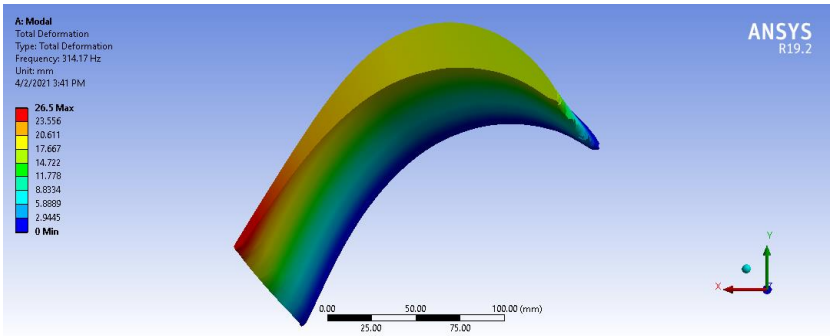

Figure 4.1: First transverse bending mode

4.2.2 Effective Mass Participation Ratio (EMPR)

Effective mass participation ratio is a constant which determines the percentage of the system's mass contributing in its dynamic response at a particular mode. The modes having a high value of participation ratio in a certain direction possess a higher dynamic response. The maximum value of participation ratio is 1. Using EMPR values from ANSYS, we can easily identify Y-modes from the other modes of the system. For instance, if at mode 1, the EMPR value in Y-direction is 1, then mode 1 is the first mode of the system in Y-direction. The mode at which the second highest value of EMPR occurs is the second mode of the system in Y-direction and so on.

For U500, we have obtained the table for EMPR for the first seven modes.

Table 4.3: EMPR values in each direction for U500

Mode	Frequency	EMPR-X	EMPR-Y	EMPR-Z
1	314.175	0.925464	1	0.000114
2	446.702	0.636309	0.495763	0.000466
3	934.814	1	0.574944	0.001595
4	1056.09	0.636863	0.022481	0.00296
5	1490.34	0.120431	0.078576	0.001803
6	1512.7	0.121409	0.028711	0.004384
7	1710.57	0.266294	0.617325	0.010187

If we observe the EMPR values in Y-direction, we can see clearly that the first Y-mode is mode 1 since it has an EMPR value of 1. Similarly, the second highest value of EMPR-Y i.e., 0.617325, occurs at mode 7, meaning that the second Y-mode is mode 7. A Y-mode is also termed as a transverse bending mode. The first and second transverse modes are identified as mode 1 and mode 7 from ANSYS.

4.2.3 Results Using Nickel Based Alloys

The same practice can be applied to the remaining materials since the blade geometry and the boundary conditions are the same. For Ni-based alloys, the first two transverse frequencies for the blade are given in table 4.4.

Table 4.4: Computational results for Nickel based alloys

S. No.	Alloy Name	First Natural Frequency (Hz)	Second Natural Frequency (Hz)
1	U-500	314.714	1708.85
2	U-700	305.58	1656.6
3	PWA-1484	215.25	1166.9
4	PWA-1480	216.12	1172.1
5	Rene N4	220.32	1194.4
6	Rene N5	217.74	1180.4
7	Rene 41	319.57	1732.4
8	CMSX-2	218.25	1183.2
9	CMSX-4	216.49	1173.6
10	IN-738	259.53	1407.51
11	IN-713	312.54	1694.3
12	IN-100	327.44	1775.1
13	IN-738 LC	286.73	1554.1
14	MAR-M246	310.008	1681.46
15	SU-263	291.78	1581.8

4.2.4 Results Using Ti-Al Based Alloys

The computational results for titanium aluminides are presented in table 4.5.

Table 4.5: Computational results for Ti-Al based alloys

S. No.	Alloy Name	First Natural Frequency (Hz)	Second Natural Frequency (Hz)
1	Ti-64	315.47	1705.5
2	Ti-811	324.33	1780.1
3	Ti-834	319.38	1729.4
4	Ti-1100	320.8	1737
5	Ti-6242	319.48	1731.2
6	Ti-685	329.2	1786
7	Ti-829	319.34	1732.5
8	Alpha-2	339.98	1844.5
9	Ti-662	306.15	1658.3
10	Ti-6246	309.51	1678.5
11	Gamma-2	409.97	2224.2
12	Ti-62s	333.81	1810.3
13	Ti-5-2.5	328.4	1781
14	Ti-679	292.32	1585.3
15	Ti-54M	306.48	1662.1

4.3 Comparing Theoretical and Computational Results

After obtaining the first and second natural frequencies of the blade using fifteen alloys each of Nickel and Ti-Al by theory and computation, the next step is to compare the results for validation. The comparison of results obtained by the two methods is presented in tables 4.6 and 4.7 for Nickel and Ti-Al based alloys respectively.

Table 4.6: Theoretical vs. computational results for Nickel based alloys

S. No.	Alloy Name	Mode	Theoretical Frequency (Hz)	Computational Frequency (Hz)	% Error
1	U-500	1	322.61	314.714	2.44
		2	2021.7597	1708.85	15.47
2	U-700	1	321.294	305.58	4.88
		2	2013.5124	1656.6	17.72
3	PWA-1484	1	226.325	215.25	4.89

		2	1418.3549	1166.9	17.73
4	PWA-1480	1	227.622	216.12	5.05
		2	1426.4831	1172.1	17.83
5	Rene N4	1	231.651	220.32	4.89
		2	1451.7325	1194.4	17.76
6	Rene N5	1	228.942	217.74	4.89
		2	1434.7526	1180.4	20
7	Rene 41	1	336.008	319.57	4.89
		2	2105.7233	1732.4	17.73
8	CMSX-2	1	229.476	218.25	4.89
		2	1438.101	1183.2	17.72
9	CMSX-4	1	227.622	216.49	4.89
		2	1426.4831	1173.6	17.73
10	IN-738	1	272.871	259.53	4.88
		2	1710.0551	1407.51	17.69
11	IN-713	1	328.619	312.54	4.89
		2	2059.4177	1694.3	17.73
12	IN-100	1	344.283	327.44	4.89
		2	2157.5874	1775.1	17.73
13	IN-738 LC	1	301.472	286.73	4.89
		2	1889.2944	1554.1	17.72
14	MAR-M246	1	326.051	310.008	4.92
		2	2034.3297	1681.46	17.71
15	SU-263	1	306.698	291.78	4.86
		2	1922.0407	1581.8	17.70

Table 4.7: Theoretical vs. computational results for Ti-Al based alloys

S. No.	**Alloy Name**	**Mode**	**Theoretical Frequency (Hz)**	**Computational Frequency (Hz)**	**% Error**
1	Ti-64	1	331.297	315.47	5.01
		2	2076.2005	1705.5	21.73

2	Ti-811	1	342.529	324.33	5.61
		2	2146.5941	1780.1	20.59
3	Ti-834	1	335.686	319.38	5.10
		2	2103.7055	1729.4	21.64
4	Ti-1100	1	337.171	320.8	5.08
		2	2113.014	1737	21.65
5	Ti-6242	1	336.055	319.48	4.93
		2	2106.0211	1731.2	17.79
6	Ti-685	1	346.436	329.2	4.98
		2	2171.076	1786	17.74
7	Ti-829	1	336.055	319.34	4.97
		2	2106.0211	1732.5	17.74
8	Alpha-2	1	357.774	339.98	4.07
		2	2242.1329	1844.5	17.73
9	Ti-662	1	321.748	306.15	4.85
		2	2016.3617	1658.3	17.76
10	Ti-6246	1	325.415	309.51	4.89
		2	2039.3415	1678.5	17.69
11	Gamma-2	1	431.433	409.97	4.97
		2	2703.7447	2224.2	17.74
12	Ti-62s	1	350.963	333.81	4.88
		2	2199.4471	1810.3	17.69
13	Ti-5-2.5	1	345.274	328.4	4.88
		2	2163.7946	1781	17.69
14	Ti-679	1	307.338	292.32	4.88
		2	1926.0574	1585.3	17.69
15	Ti-54M	1	322.226	306.48	4.89
		2	2019.3555	1581.8	17.69

For all the available materials, we can see that the first transverse mode shows the best agreement with analytical results with an error percentage of almost 5%. However, this error percentage increases to about 17% for the second transverse mode. The reason for this is due to increase in discretization error for higher modes. Due to the increased error, a much finer mesh

setting would be needed to capture the results for the second mode with good accuracy. In our study, we only need to compare the fundamental frequencies of the materials under consideration. Therefore, we don't need to spend a great deal of computational resources on the second mode since materials having a higher fundamental frequency would automatically have a higher second natural frequency as well.

Figure 4.2 shows a graphical comparison between first and second modes for U500 and Ti-64. The increasing error for second mode can be shown by lines diverging more at mode 2.

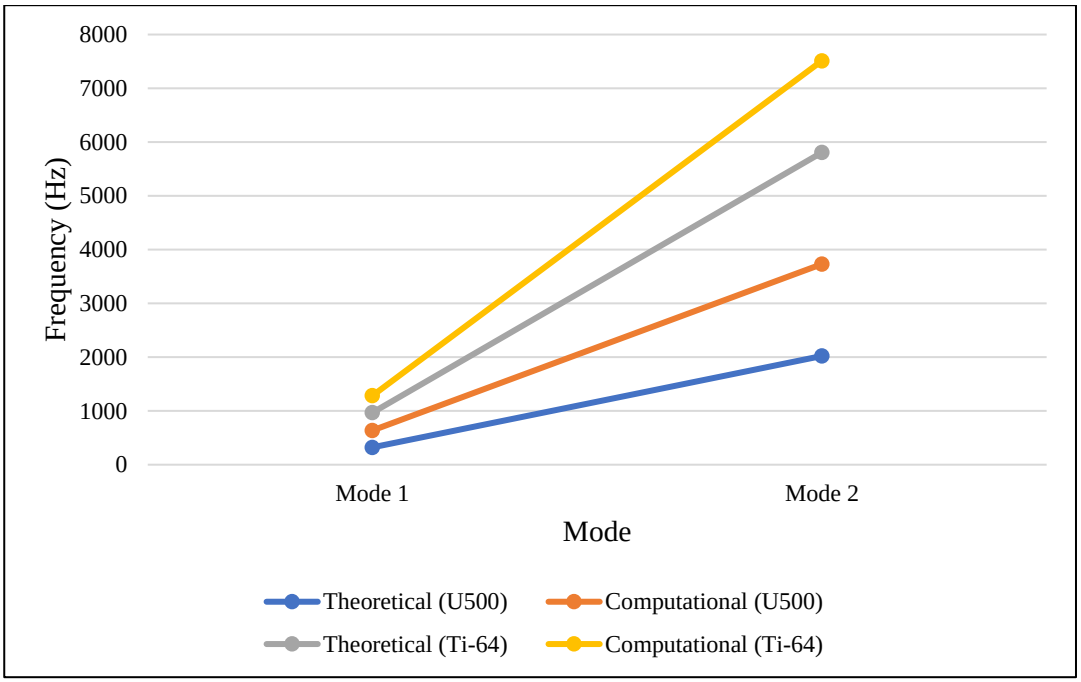

Figure 4.2: Comparison of Theory and Computation (For U500 and Ti64)

4.4 Material Comparison and Selection

The comparison of the materials studied so far and the selection of the most suitable material for an LPT blade will be based on the following criteria, as already discussed in the previous chapters:

- **High Fundamental Frequency:** Although both the first and second natural frequencies of the LPT blade have been obtained for all the materials under study, only the first natural frequency or the fundamental frequency of the blade in the transverse bending direction will be considered in material comparison. This is because the first mode of vibration is

the most critical and the blade is most likely to resonate at its lowest natural frequency. Thus, the most suitable blade material will be the one for which the blade's fundamental frequency is the highest, with the other criteria satisfied. The fundamental frequencies obtained from ANSYS will be used in the comparison.

- **Low Mass:** Since one of the goals of this research is to reduce the LPT weight by means of suitable material selection, the most suitable blade material will be the one for which the blade's mass is the lowest, with the other criteria satisfied. The blade mass obtained for each material from ANSYS will be used in the comparison.
- **High Stiffness:** To prevent rigorous blade vibrations and blade flutter, the LPT blades should be made stiffer. Therefore, the most suitable blade material will be the one for which the blade's stiffness is the highest, with the other criteria satisfied. Blade stiffness for each material will be calculated from the following relation:

$$k = \omega^2 m$$

The most ideal situation would be for one single material to satisfy all the criteria. But it is neither necessary nor likely for one material to satisfy all the selection criteria. For example, a high frequency and greater mass equate to higher blade stiffness, satisfying two (high frequency and high stiffness) criteria but violating one (low mass) criterion. Therefore, a thorough comparison of the materials shall be made to select the material that satisfies a majority of the suitability criteria with acceptable margins. First of all, a comparison will be made among the Nickel alloys to select the most suitable Nickel alloy. The same will be done for Ti-Al based alloys and the most suitable Ti-Al alloy will be selected. Finally, the most suitable Nickel based alloy will be compared with the most suitable Ti-Al based alloy to make the final selection of the most suitable LPT blade material.

4.4.1 The Most Suitable Nickel Based Alloy

The fundamental frequency, mass and stiffness of the T106 blade for each Nickel based alloy is presented in table 4.8.

Table 4.8: Blade fundamental frequency, mass and stiffness using Nickel alloys

S. No.	Alloy Name	Fundamental Frequency (Hz)	Mass (kg)	Stiffness (MN/m)
1	U-500	314.714	10.08	39.4
2	U-700	305.58	9.96	36.7
3	PWA-1484	215.25	11.388	20.8
4	PWA-1480	216.122	11.26	20.8
5	Rene N4	220.32	10.871	20.8
6	Rene N5	217.74	11.13	20.8
7	Rene 41	319.57	10.677	43.1
8	CMSX-2	218.25	11.078	20.8
9	CMSX-4	216.49	11.259	20.8
10	IN-738	259.538	11.05	29.4
11	IN-713	312.54	10.24	39.5
12	IN-100	327.44	10.03	42.5
13	IN-738 LC	286.73	10.214	33.2
14	MAR-M246	310.008	10.92	41.4
15	SU-263	291.78	10.522	35.4

For clarity, the comparison is made in the bar chart presented in figure 4.3.

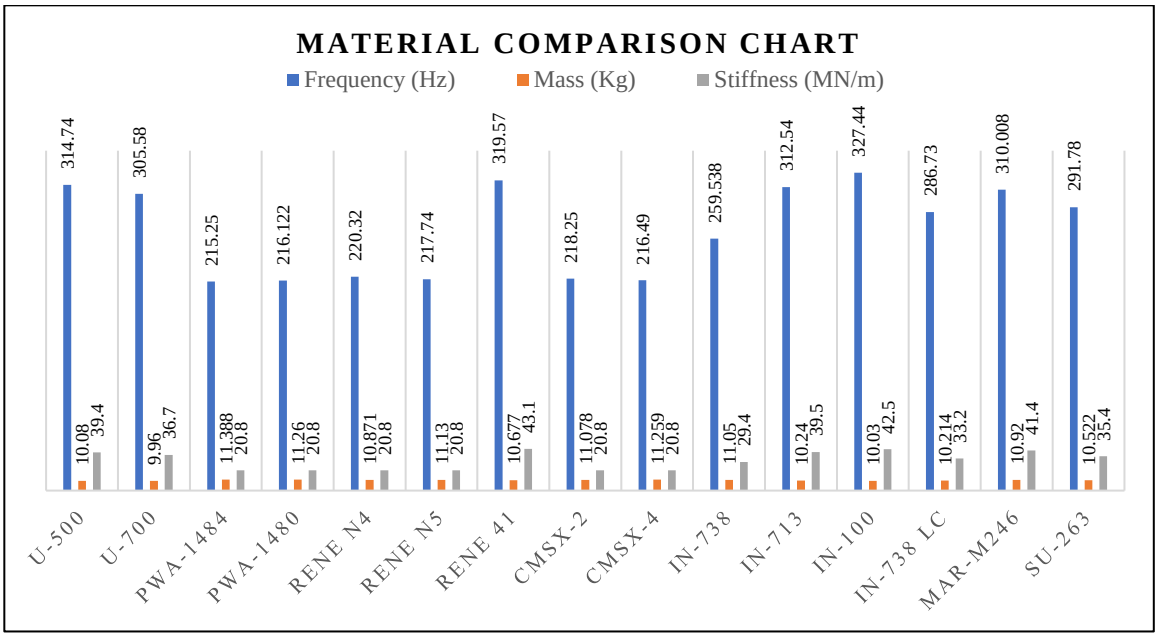

Figure 4.3: Comparison of Nickel Based Alloys

Amongst all the Ni-based alloys, our goal is to pick a material that satisfies maximum number of parameters (i.e., mass, stiffness and natural frequency). On comparison, we find out that IN-100 is a material which, when compared to any other Ni-based material in our study, stands superior in 2 out of 3 parameters. It possesses the highest natural frequency, second highest stiffness and second lowest mass. Therefore, the optimal choice for the most suitable Ni-based alloy stands out to be IN-100.

4.4.2 The Most Suitable Ti-Al Alloy

The fundamental frequency, mass and stiffness of the T106 blade for each Ti-Al based alloy is presented in table 4.9.

Table 4.9: Blade fundamental frequency, mass and stiffness using Ti-Al alloys

S. No.	Alloy Name	Fundamental Frequency (Hz)	Mass (kg)	Stiffness (MN/m)
1	Ti-64	315.47	5.73	22.5
2	Ti-811	324.33	5.65	23.5
3	Ti-834	319.38	5.89	23.7
4	Ti-1100	320.8	5.84	23.7
5	Ti-6242	319.48	5.8714	23.7
6	Ti-685	329.2	5.755	24.6
7	Ti-829	319.34	5.8714	23.6
8	Alpha-2	339.98	6.2594	28.6
9	Ti-662	306.15	5.8714	21.7
10	Ti-6246	309.51	6.0007	22.7
11	Gamma-2	409.97	5.2248	34.7
12	Ti-62s	333.81	5.7421	25.3
13	Ti-5-2.5	328.4	5.7938	24.7
14	Ti-679	292.32	6.2594	21.1
15	Ti-54M	306.48	6.0136	22.3

For clarity, the comparison is made in the bar chart presented in figure 4.4.

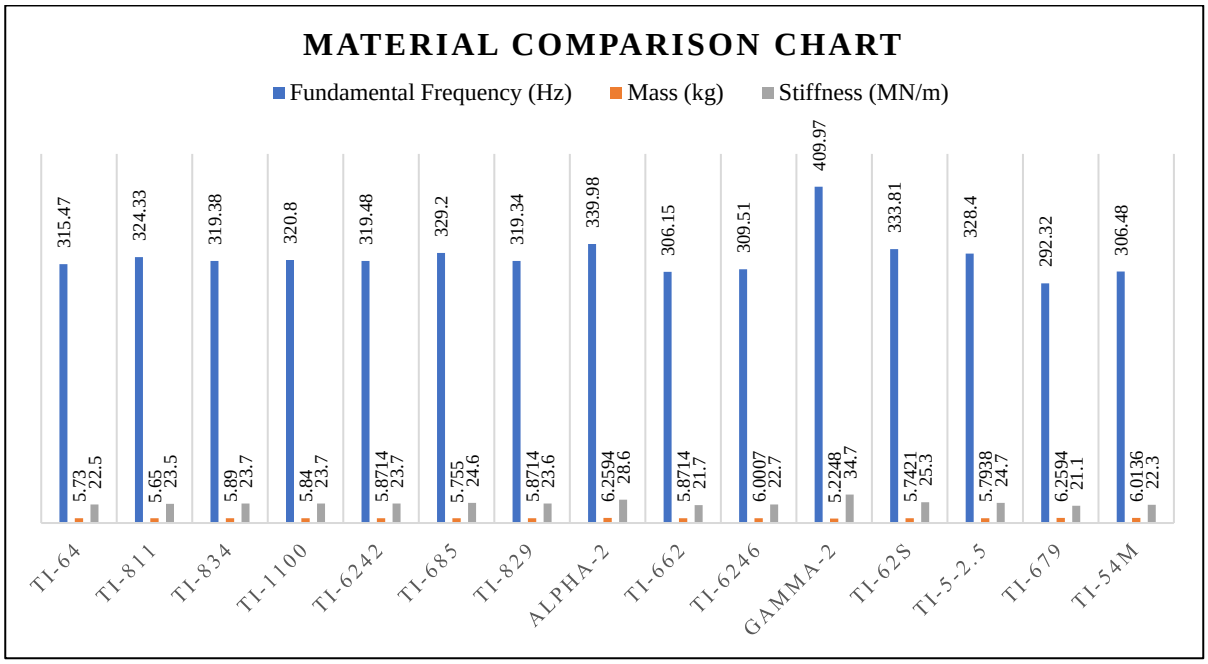

Figure 4.4: Comparison of Ti-Al alloys

It can be seen from figure 4.4 that Gamma-2 alloy has the highest fundamental frequency of 409.97 Hz, lowest blade mass of 5.2248 kg and highest blade stiffness of 34.7 MN/m among all the studies Ti-Al alloys. Therefore, Gamma-2 is the most suitable Ti-Al alloy and is selected for final comparison with the most suitable Nickel based alloy i.e., IN-100.

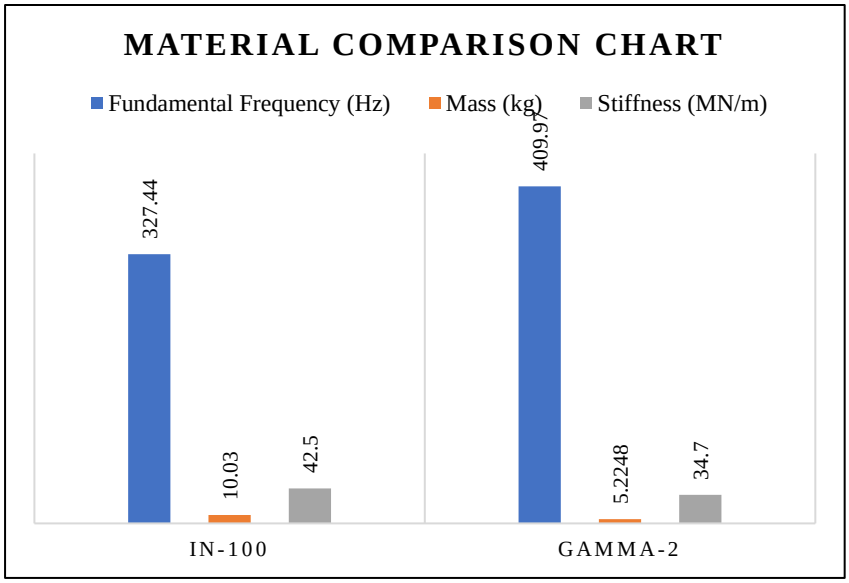

Figure 4.5: Comparison of IN-100 and Gamma-2

It can be seen in figure 4.5 that Gamma-2 satisfies two out of the three selection criteria i.e., higher fundamental frequency and lower mass. On the other hand, IN-100 satisfies only one of the three criteria i.e., higher blade stiffness. Looking at the difference margins, selecting Gamma-2 over IN-100 achieves:

- 25.2% increase in blade fundamental frequency
- 47.9% reduction in blade mass
- 18.4% reduction in blade stiffness

Therefore, Gamma-2 satisfies a majority of the selection criteria with acceptable margins. By selecting Gamma-2 over IN-100, the blade mass is nearly halved. This means that if Gamma-2 is employed in various parts of an aero-engine replacing Nickel based alloys, there will be a considerable reduction in the engine weight resulting in increased fuel efficiency and increased payload capacity.

4.5 Calculation of Modal Parameters

As explained in the previous sections, modal parameters help us model the continuous physical system into a discrete mass spring system so that structural modifications can be performed as per requirement. In our case, local structure modification isn't feasible since it will alter the blade design. That is why we performed a comparative study to choose the material that suits our requirement. Once the material has been chosen, we shall now determine its modal parameters so that the structure can be analyzed in the modal domain, which is in fact the heart of modal analysis.

4.5.1 IN-100

Amongst the Ni-based alloys, IN-100 was chosen as the most suitable material due to high natural frequency and a comparatively lesser mass. The modal parameters of IN-100 are provided in the following table

Table 4.10: Modal parameters for IN-100

Mode	Frequency (Hz)	Mass [kg]	Stiffness [N/m]	Damping [Ns/m]	Damping ratio ζ
1	327.44	2.54E-03	1.07E+04	7.03E-03	6.71E-04
2	1775.11	1.36E-03	1.70E+05	1.51E-02	4.95E-04

The modal parameters have been obtained for the first two modes since these modes show a relatively close agreement with analytical results. By inspecting the values, we can see that the modal stiffness increases while the modal mass decreases at the second mode. This shows an example of a stiffness dominant system.

The values of modal mass were determined using analytical relations in provided in M. H. Richardson's work [14]. They were also compared with the modal mass value obtained from ANSYS in table 4.11. The values of modal mass agree with each other to a decent extent as displayed in the table.

Table 4.11: Comparison of modal masses for IN-100

Mode	Calculated mass (kg)	Computational mass (kg)	Error %
1	2.54E-03	2.44E-03	4.20
2	1.36E-03	1.29E-03	5.79

4.5.1.1 Mode Shapes

The mode shapes for first and second transverse bending modes are provided in the figures.

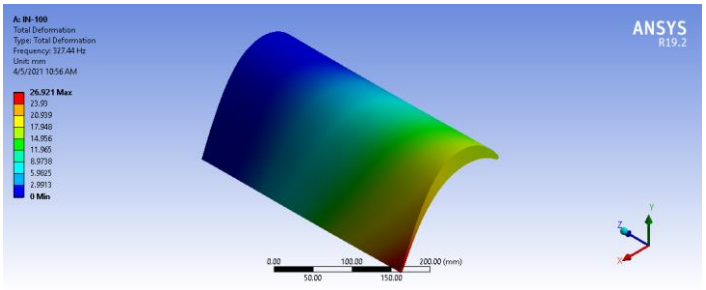

Figure 4.6: First mode shape for IN-100

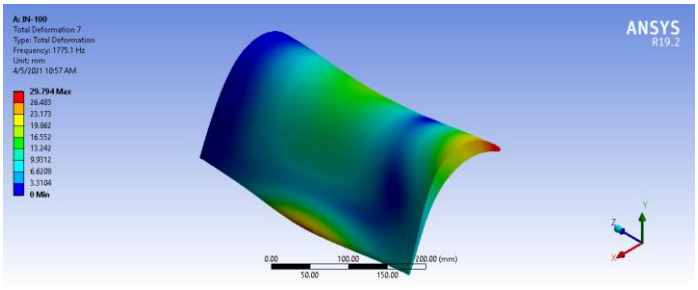

Figure 4.7: Second mode shape for IN-100

4.5.1.2 Curve Fitting on MATLAB

The modal parameters provided in table 4.10 were plotted in MATLAB using the transfer function approach. The plot in figure 4.8 describes the response of the system's transfer function$\frac{X(s)}{F(s)} = T(s)$. This is known as the transfer function approach.

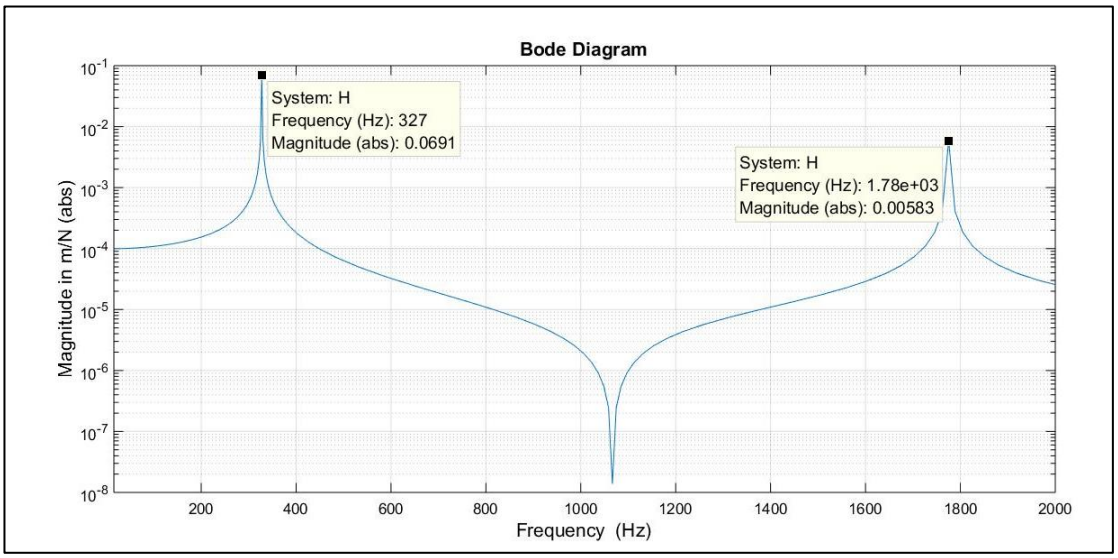

Figure 4.8: Frequency response of the system using Matlab

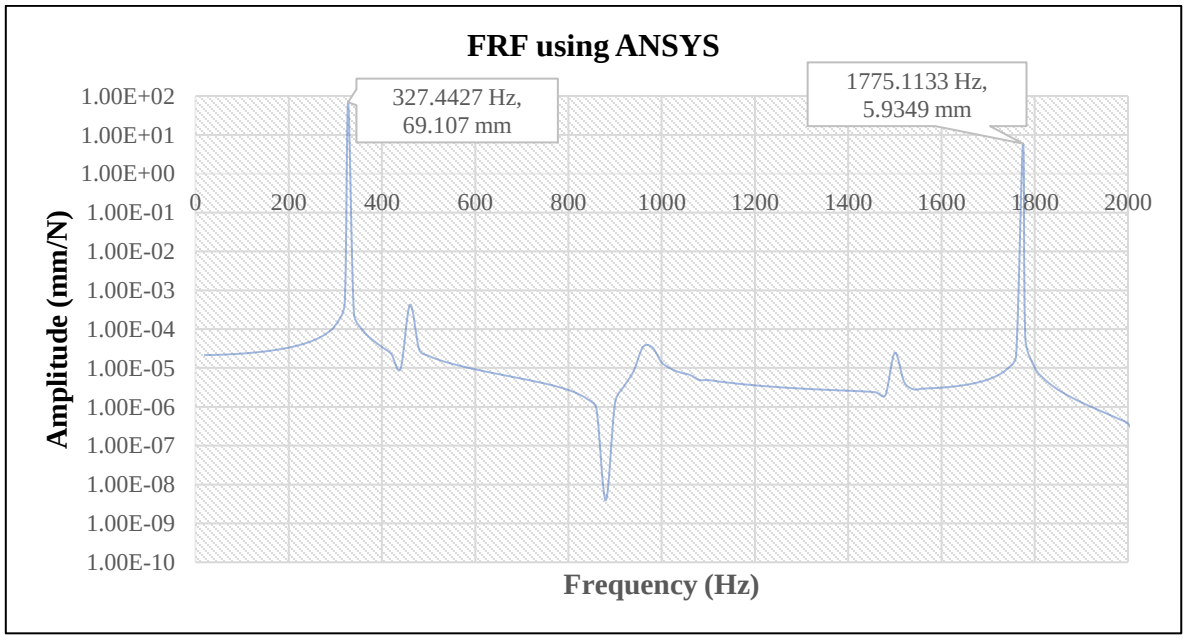

Figure 4.9: Frequency response plot from ANSYS harmonic response

Whereas in harmonic response, the system's response x(t) under a harmonic excitation is determined as a solution to Eq. (1). This time domain response is converted into a frequency domain response by applying Fast Fourier Transform. In ANSYS, we can obtain our system's harmonic displacement in the form of a frequency response function which is plotted in figure 4.9.

By inspecting the plots and their peak values, we can conclude that the curve fitting has been successfully performed. The modal parameters thus calculated are correct. Using these modal parameters and the mathematical model, one can modify the structure's design to obtain the desired natural frequency or response.

4.5.2 Gamma-2-Ti

For Gamma-2-Ti, the modal parameters determined are provided in the following table

Table 4.12: Modal parameters of Gamma-2-Ti

Mode	Frequency (Hz)	Mass [kg]	Stiffness [N/m]	Damping [Ns/m]	Damping ratio ζ
1	409.97	1.24E-03	8.27E+03	2.86E-03	4.46E-04
2	2224.24	7.15E-04	1.39E+05	2.23E-03	1.11E-04

The table shows that the significance of the second mode is quite higher than that of the first mode. This will further be confirmed from the FRF plot in which the second peak lies lower than the first peak due to the reason that the second mode is stiffer than the first mode. This is also an example of a stiffness dominant system. A comparison between modal masses from ANSYS and theory is shown in table 4.13.

Table 4.13: Comparison of modal mass for Gamma-2-Ti

Mode	Calculated mass (kg)	Computational mass (kg)	Error %
1	1.24E-03	1.28E-03	2.53
2	7.15E-04	6.66E-04	7.40

4.5.2.1 Mode Shapes

Mode shapes for first and second transverse modes will be similar to IN-100 and are displayed as follows:

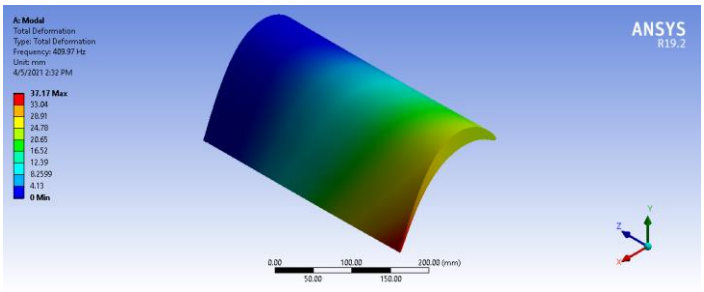

Figure 4.8: First transverse bending mode (Gamma-2-Ti)

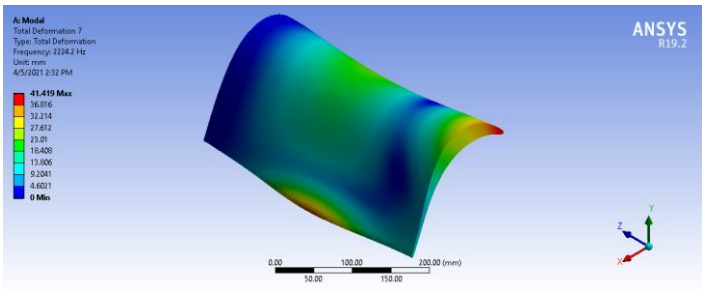

Figure 4.9: Second transverse bending mode (Gamma-2-Ti)

4.5.2.2 Curve Fitting on MATLB

By using the obtained modal parameters in Table 4.12, we can write the transfer function of our system as described in Eq. (14). The magnitude of this plot determines the receptance of our system and is drawn on MATLAB as shown in figure 4.13.

From ANSYS, the harmonic response data corresponds to the plot shown in figure 4.12. By comparing these plots and the peak values, we can check that they are consistent with each other. Hence, our modal parameters are correct since they show a decent agreement with the computationally obtained FRFs.

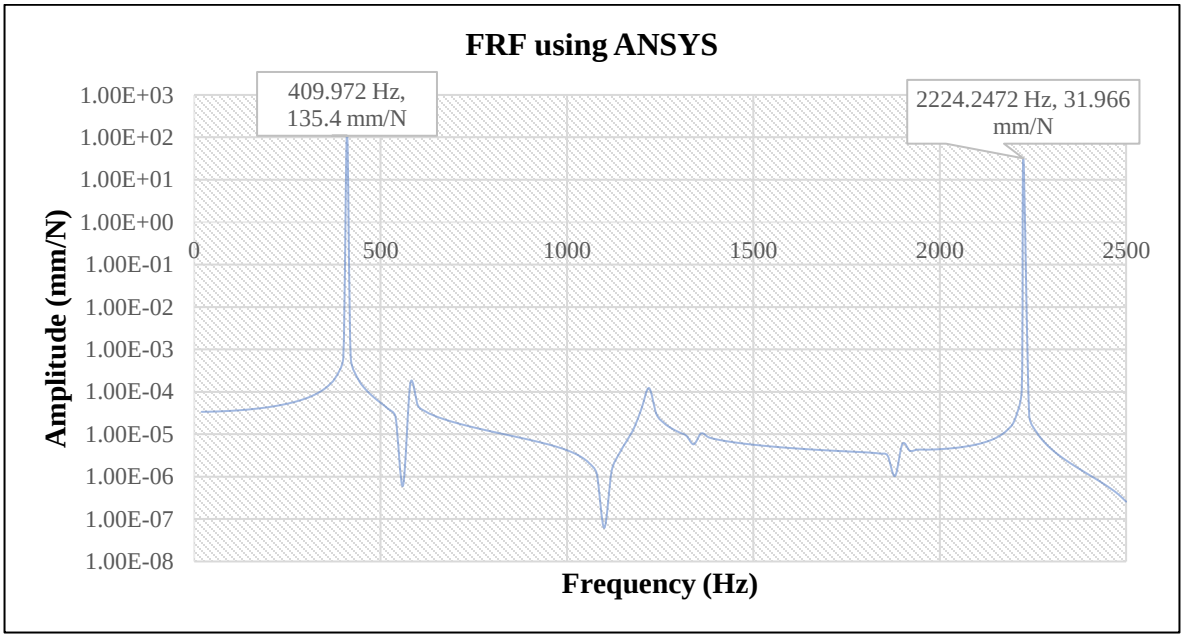

Figure 4.12: Frequency response plot from ANSYS harmonic response

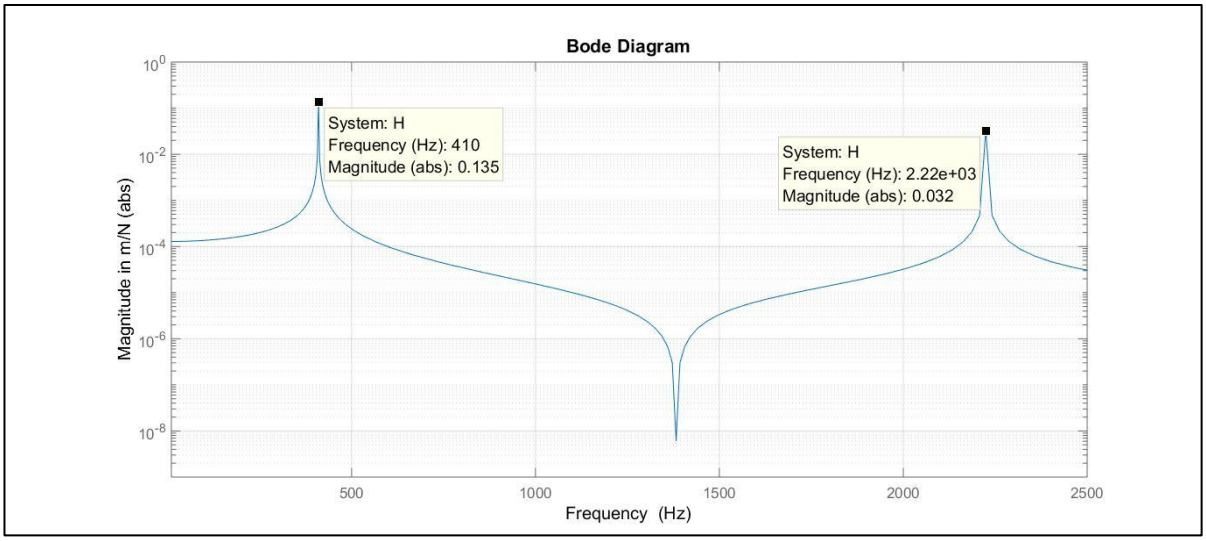

Figure 4.13: Frequency response of the system on MATLAB

4.5.3 Comparison of Response between IN-100 and Gamma-2-Ti

Now if we compare the FRFs for both IN-100 and Gamma-2-Ti, we can see that the IN-100 displays a lower amplitude at resonance when compared with Gamma-2-Ti. Furthermore, the area under a peak which corresponds to damping ratio is also higher for IN-100 as compared to

Gamma-2-Ti. However, the key difference which makes Gamma-2-Ti a better choice as compared to IN-100 is its fundamental frequency which is about 20% greater than that of IN-100. If we increase the fundamental frequency, we lower the chances of our blade undergoing resonance at a comparatively lower frequency. Also, amplitude of vibration can always be controlled by adjusting the load on the turbine, whereas controlling the natural frequency requires local structural modifications. We have accomplished this goal by making a comparison among the already used materials in turbomachinery and based on the results, we infer that Gamma-2-Ti would be the most suitable material choice for use in a low-pressure turbine.

CHAPTER 5: CONCLUSION AND RECOMMENDATION

5.1 Conclusion

5.1.1 Analysis Results

Hence, we performed computational modal analysis of a low-pressure turbine blade i.e., T106 blade using Ni-based and Ti-Al based alloys. Our objective was to safeguard the blade against vibrations by improving its dynamic characteristics and at the same time, keep the blade's mass to a minimum so that the overall weight of the LPT stage can be reduced. To accomplish this objective, we could either modify the blade's design which was not feasible and would possibly affect the LPT's performance, or we could choose a blade material under which the blade would exhibit our desired characteristics. The latter was our approach in which we performed computational modal analysis of the blade and calculated its natural frequencies, mass and stiffness. The data was obtained for both Nickel and Ti-Al based alloys. To validate the computation, we used natural frequency results from the Euler Bernoulli beam theory under fixed free boundary condition. Amongst the Ni-based alloy, IN-100 was chosen as the most suitable blade material. Whereas, Gamma-2-Ti was chosen as the most suitable alloy (due to its highest frequency and stiffness, and least mass) among Ti-Al alloys. Furthermore, a harmonic analysis of the chosen materials was also performed to investigate their dynamic properties in the form of frequency response plots. The frequency response plots for displacement were used to obtain the modal parameters of the blade for the selected materials. The modal parameters were then used to plot the system's amplitude as a function of its frequency and check its correspondence with the FRF plots from ANSYS.

5.1.2 Material Selection

In order to make the final choice regarding the most suitable blade material, IN-100 and Gamma-2-Ti were compared with each other. Although IN-100 provided us with a slightly higher blade stiffness, however, it was traded off for a much higher increase in natural frequency and almost half the reduction in mass by employing Gamma-2-Ti. Hence, based on our criteria, we could clearly say that Gamm-2-Ti was the most suitable material for use in the LPT blade, which does only prevent the blade from resonating at lower frequencies, but also reduces the mass of the

stage by a half. However, we should also assert that use of Titanium alloys is more costly as compared to Nickel due to the expensive manufacturing techniques of Ti-Al alloys.

5.1.3 The Future of Titanium Aluminides:

Titanium aluminides with their low densities started interesting the aerospace industry researchers as early as the 1970s, but it took three decades of extensive research and development for Ti-Al based alloys to reach the level of maturity at which commercial aircraft manufacturers viewed them as suitable candidates for replacing Nickel based alloys in critical rotating components of jet engines. Incorporation of Ti-Al blades in the last two stages of the seven-stage low pressure turbine in GEnX 787 jet engine (General Electric) to achieve significant weight savings over conventional Nickel alloys [15] proves their technological maturity as high-temperature structural materials.

Titanium Aluminides are now viewed as bright future prospects for replacing high density Nickel based alloys in rotating components of jet engines, however, the biggest hurdle in the way of their widespread commercial implementation today is that they are difficult to manufacture. Titanium Aluminides are difficult to form because of their low ductility. Figures 5.1, 5.2 and 5.3 show that while Titanium Aluminides have higher specific modulus and specific strength compared to Nickel based super-alloys and alloy Steel between room temperature and 800 ^{o}C, they have a much lower percentage elongation at room temperature [10].

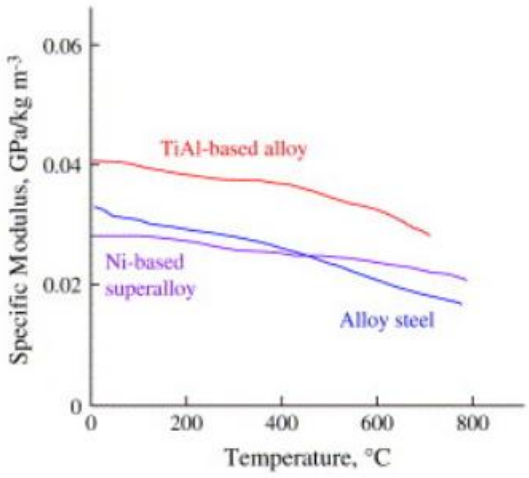

Figure 5.1: Specific modulus vs. temperature of different alloy classes [10]

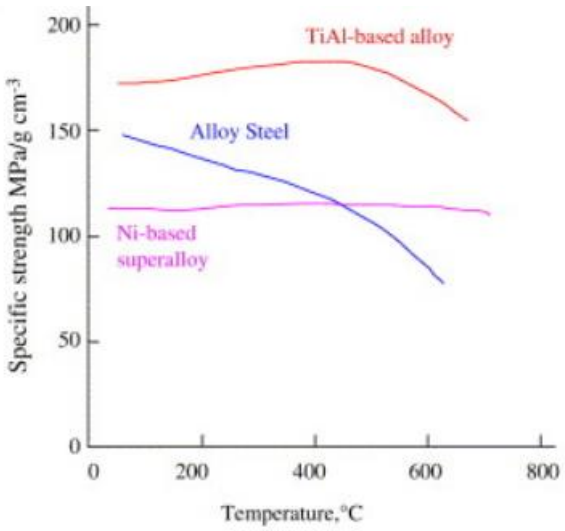

Figure 5.2: Specific strength vs. temperature of different alloy classes [10]

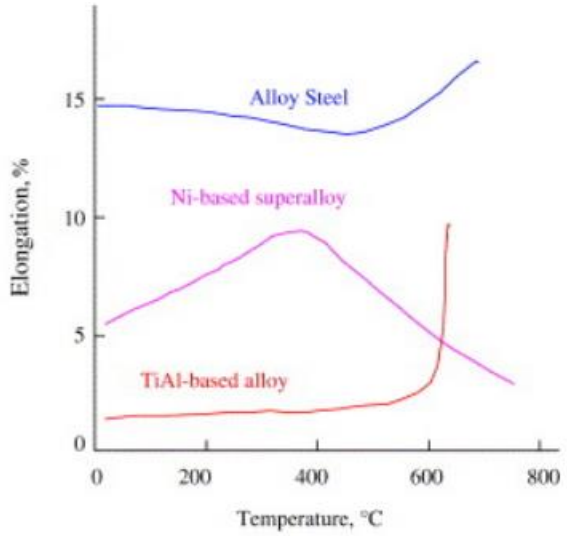

Figure 5.3: % elongation vs. temperature of different alloy classes [10]

Although conventional methods of forging and extrusion have been used to develop smaller parts from Titanium Aluminides for engine testing by Rolls-Royce, bigger components with intricate geometries could not be successfully formed [10].

Today, commercial aircraft manufacturing companies are focused on the successful manufacturing of intricate engine parts from Titanium Aluminides and metal additive manufacturing techniques have showed encouraging results in this regard. In additive

manufacturing, parts are joined/solidified from a powder feedstock. Powder bed fusion (PBF) is an AM technique that uses electron beam melting (EBM) and laser powder bed fusion (LPBF) to create 3D components in a layer-wise manner from the powder feedstock. PBF allows the creation of complex parts monolithically, and therefore, can be used to manufacture intricate parts from Titanium Aluminides with reduced manufacturing and maintenance costs, also avoiding material wastage [11]. General Electric has manufactured more than 40,000 LPT blades using AM to explore this near-net-shape manufacturing technique as an alternative for the previously used gravity casting plus machining to manufacture LPT blades for Boeing 787. These 40,000 LPT blades were manufactured for GEnX^{TM} 1B (Boeing 787) and GEnX^{TM} 2B (747-8) [16].

Additive manufacturing is winning the acceptance of commercial aircraft engine manufacturers and is being viewed as a high potential technique to manufacture products with complex geometries [17]. Newer approaches such as pre-heating in the LPBF process [18] and the use of third generation Ti-Al based alloys (TNM) with β-stabilizing elements to manufacture crack-free Ti-Al [19] components are showing promise, and the goal of mass implementation of Ti-Al based components in aero-engines is getting closer every day.

With advanced manufacturing techniques and approaches being applied to the production of components from Ti-Al based alloys, these alloys will soon replace Nickel based alloys in various aero-engine parts, including the LPT blades. The replacement of Nickel alloys by Gamma-2-Ti as LPT blade material will increase the blade fundamental frequency reducing the chances of blade failure due to vibration and considerably reduce the turbine weight. The use of Ti-Al based alloys is certainly not limited to LPT only, and their application in various other engine components will pay off with a reduction in the engine weight, reduction in emissions and increased fuel efficiency [16].

REFERENCES

[1] R. S. Peterhouse, "The effects of wakes on seperating boundary layer in low pressure turbine blades," Cambridge University Engineering Department, Cambridge, 2002.

[2] N. R. Muktinutalapati, "Materials for Gas Turbines - An Overview," in *Advances in Gas Turbine Technology*, Vellore, pp. 293-314.

[3] S. Rao, "Continous Systems," in *Mechanical Vibrations, 6th edition*, Pearson, pp. 748-822.

[4] R. Stieger and H. Hodson, "The transition mechanism of highly loaded LP turbine blades," in *ASME Turbo Expo 2003*, Atlanta, 2003.

[5] M. B. Ali Demirtas, "Free vibration analysis of an aircraft wing by considering as a cantilever beam," *Selcuk University Journal of Engineering Science & Technology*, vol. 7, pp. 12-21, 2019.

[6] J. K. Sharma, "Theoretical and Experimental Modal Analysis of a Beam," in *Engineering Vibration, Communication and Information Processing*, Singapore, Springer, Singapore, 2019, pp. 177-186.

[7] P. S. T. Ashish R. Sonawane, "Modal Analysis of Single Rectangular Cantilever Plate by Mathematically, FEA and Experimental," *International Research Journal of Engineering and Technology (IRJET)*, vol. 4, no. 8, 2017.

[8] A. E. I. G. O. A. Oghenefejiro E. Efe-Ononeme, "MODAL ANALYSIS OF CONVENTIONAL GAS TURBINE BLADE MATERIALS (UDIMET 500 AND IN-738) FOR INDUSTRIAL APPLICATIONS," *Journal of Engineering Technology and Applied Sciences*, vol. 3, no. 2, pp. 119-133, 2018.

[9] T. Okura, "Materials for Aircraft Engines," ASEN 5063 Aircraft Propulsion Report.

[10] X. Wu, Review of Alloy Process Development of TiAl Alloys, 10-11 ed., vol. 14, Intermetallics, 2006, pp. 1114-1122.

[11] T. C. Dzogbewu, Additive Manufacturing of Ti-Al Based Alloys, Manufacturing Rev. 7, 35, 2020.

[12] S. P. Chaphalker, S. N. Khetre and A. M. Meshram, "Modal analysis of cantilever beam structure using Finite Element Analysis and Experimental Analysis," *American Journal of Engineering Research*, vol. 4, no. 10, pp. 178-185, 2015.

[13] S. Rao, "Quality Factor and Bandwidth," in *Mechanical Vibrations, 6th edition*, Pearson, pp. 316-317.

[14] M. H. Richardson, *Derivation of Mass, Stiffness and Damping Parameters From Experimental Modal Data,* 1977.

[15] S. F. Clark, 787 Propulsion System, Aero QTR. 3, 2012, pp. 5-13.

[16] B. P. Bewlay, M. Weimer and T. Kelly, The Science, Technology, and Implementation of TiAl Alloys in Commercial Aircraft Engines, MRS Online Proceedings Library 1516, 2013, pp. 49-58.

[17] S. A. Raji, A. P. I. Popoola and S. L. Pityana, Laser Based Additive Manufacturing Technology for Fabrication of Titanium Aluminides Based-Composites in Aerospace Component Applications, Aerodynamics, IntechOpen, 2019.

[18] L. Caprio, A. G. Demir and G. Chiari, Defect-free Laser Powder Bed Fusion of Ti-48Al-2Cr-2Nb with a High Temperature Inductive Preheating System, J. Phys., Photonics 024001, 2020.

[19] L. Lober, F. P. Shimansky and U. Kuehn, Selective Laser Melting of a Beta-Solidifying TNM-B1 Titanium Aluminide Alloy, Journal of Materials Processing Technology, Elsevier, 2014.

[20] S. Rao, "Harmonically Excited Vibrations," in *Mechanical Vibrations Sixth Edition*, pp. 302-304.

[21] S. H. Parbant Singh, "Modal Analysis of Bearing Using Finite Element Method," *Journal of Emerging Technologies and Innovative Research,* vol. 6, no. 6, 2019.

[22] P. Mirji, "Modal Analysis of a Square Plate with Different Shape Cut Out," *International Journal of Trend in Scientific Research and Development (IJTSRD),* vol. 3, no. 3, pp. 456-461, 2019.

[23] M. N. M. Sai Kiran, "Structural and Modal analysis of Air craft wing," *International Journal of Science & Engineering Development Research - IJSDR,* vol. 3, no. 12, 2018.

[24] P. Lengvarsky, J. Bocko and M. Hagara, "Modal analysis of Titan cantilever beam using Ansys and Solidworks," *American Journal of Mechanical Engineering,* vol. 1, pp. 271-275, 2013.

[25] Z.-F. F. Jimin He, "Modal Analysis of a damped MDOF System," in *Modal Analysis*, 2001, pp. 108-137.

[26] A. Mukherjee and A. Gosai, "Determination of Natural Frequency of Euler's beam using analytical and finite element method," Kolkata, 2010.

[27] P. K. M. ,. S. M. Santosh Kumar Tripathy, "Model Analysis of Variation of Taper Angle for Cantilever and Simply Supported Beam," *International Journal of Innovative Research in Science, Engineering and Technology,* vol. 4, no. 11, 2015.

[28] L. K. Bhagi, P. Gupta and V. Rastogi, ""A Brief Review on Failure of Turbine Blades"," in *Smart Technologies for Mechanical Engineering*, Delhi, 2013.

[29] W. Chen and Z. Li, "Additive Manufacturing of Titanium Aluminides" in Additive Manufacturing for the Aerospace Industry, 2019, pp. 235-263.

[30] T. Hariprasad, M. V. Sagar and D. M. Kumari, ""Failure Analysis of Last Stage Low Pressure Steam Turbine Blade"," *International Journal for Research in Applied Science & Engineering Technology (IJRASET),* vol. 5, no. 12, 2017.

[31] S. A. Khan, I. Arif and M. U. Safdar, "Determination and Comparison of Modal Parameters of a High Lifting Low Pressure Turbine Blade Under Ni-Based Superalloys Using Computational Modal Analysis" in 2021 International Bhurban Conference on Applied Sciences and Technologies (IBCAST), Islamabad: IEEE, 2021, pp. 169-176.

[32] J. Lapin, "TiAl-Based Alloys: Present Status and Future Perspectives", Hradec NAD Moravici. 19., 2009.

[33] R. F. Orsagh and M. J. Roemer, "Examination of Successful Modal Analysis Techniques Used for Blade-Disk Assemblies", 125 Tech Park Drive Rochester, New York 14623 : Impact Technologies, LLC.

[34] M. -T. Perez-Prado and M. E. Kassner, "Creep of Intermetallics" in Fundamentals of Creep in Metals and Alloys, 3 ed., Butterworth-Heinemann, 2015, pp. 189-232.

[35] J. C. Williams and R. R. Boyer, "Opportunities and Issues in the Application of Titanium Alloys for Aerospace Components" in Metals, vol. 10, MDPI, 2020.

[36] M. J. Iqbal, G. Y. Chohan, S. Khusnood and M. A. Khan, ""Vibration Analysis of Gas Turbine Blade Using FEM"," Doctor AQ Khan Research Labs, Islamabad, 2003.